Mechanical Systems and Signal Processing 189 (2023) 110095

Contents lists available at ScienceDirect

Mechanical Systems and Signal Processing

journal homepage: www.elsevier.com/locate/ymssp

Instantaneous amplitude and phase signal modeling for harmonic removal in wind turbines

Miroslav Zivanovic [a,c,*], Aitor Plaza [b], Xabier Iriarte [b,c], Alfonso Carlosena [a,c]

[a] Dept. Ingeniería Eléctrica, Electrónica y de Comunicación, Universidad Pública de Navarra, Campus Arrosadía, 31006 Pamplona, Spain
[b] Dept. Ingeniería, Universidad Pública de Navarra, Campus Arrosadía, 31006 Pamplona, Spain
[c] ISC-Institute of Smart Cities, Universidad Pública de Navarra, Campus Arrosadía, 31006 Pamplona, Spain

ARTICLE INFO

Keywords:
Wind turbine
Harmonic disturbances
Non-stationary signal modeling
Structural Health Monitoring (SHM)
Operational Modal Analysis (OMA)
Rotary machinery

ABSTRACT

We present a novel approach to harmonic disturbance removal in single-channel wind turbine acceleration data by means of time-variant signal modeling. Harmonics are conceived as a set of quasi-stationary sinusoids whose instantaneous amplitude and phase vary slowly and continuously in a short-time analysis frame. These non-stationarities in the harmonics are modeled by low-degree time polynomials whose coefficients capture the instantaneous dynamics of the corresponding waveforms. The model is linear-in-parameters and is straightforwardly estimated by the linear least-squares algorithm. Estimates from contiguous analysis frames are further combined in the overlap-add fashion in order to yield overall harmonic disturbance waveform and its removal from the data. The algorithm performance analysis, in terms of input parameter sensitivity and comparison against three state-of-the-art methods, has been carried out with synthetic signals. Further model validation has been accomplished through real-world signals and stabilization diagrams, which are a standard tool for determining modal parameters in many time-domain modal identification algorithms. The results show that the proposed method exhibits a robust performance particularly when only the average rotational speed is known, as is often the case for stand-alone sensors which typically carry out data pre-processing for structural health monitoring. Moreover, for real-world analysis scenarios, we show that the proposed method delivers consistent vibration mode parameter estimates, which can straightforwardly be used for structural health monitoring.

1. Introduction

Operational Modal Analysis (OMA) is a generic name for output-only system identification strategies, which provide characterization of large structures – wind turbines (WT), bridges, buildings, etc. – from vibration signals under operating conditions. There are two main reasons why the application of conventional modal analysis techniques, requiring the use of well-controlled excitation signals, is impossible in those cases. First, the size of the structures does not allow the excitation with the required energy, for either stationary or impulsive signals. Second, the characteristics of the structure under test are not the same under static or operating conditions due for instance to aeroelastic effects. OMA techniques, formerly known also as Natural Excitation Techniques (NExT),

* Corresponding author at: ISC-Institute of Smart Cities, Universidad Pública de Navarra, Campus Arrosadía, 31006 Pamplona, Spain.
E-mail addresses: miro@unavarra.es (M. Zivanovic), aitor.plaza@unavarra.es (A. Plaza), xabier.iriarte@unavarra.es (X. Iriarte), alfonso.carlosena@unavarra.es (A. Carlosena).

https://doi.org/10.1016/j.ymssp.2023.110095
Received 3 November 2021; Received in revised form 15 December 2022; Accepted 2 January 2023
Available online 6 January 2023

make use of natural excitation signals such as wind, waves, rain or road traffic as the only, or even the most adequate, excitation signals available.

An extensive overview of the principal OMA techniques in the context of structural health monitoring (SHM) is given in [1], which include time and frequency domain, parametric and non-parametric procedures. Whatever the case, OMA assumes routinely that the system input is the realization of a stochastic process which can be modelled by white noise [2]. However, this is not always the case, particularly for structures containing rotating parts such as turbines of any kind or gearboxes. In these cases, measured output signals contain a mixture of the structure response and harmonic perturbations in the frequencies of the rotating parts and their higher order harmonics.

If not properly taken into account, those disturbances may seriously hamper the OMA procedure by introducing bias in the estimation of the natural frequencies or identifying the harmonics as structural modes, particularly when mode frequencies are close to some harmonic [3]. This happens in wind turbines, but a number of applications [4–6] are reported where harmonics constitute a severe limitation for the proper application of OMA techniques to estimate modal frequencies, damping and mode shapes. It is interesting to note how historically the inception of OMA was with vertical wind turbines [7] while in today's horizontal wind turbines the problem of harmonic interference has hardly been dealt with until recently.

There are a few review papers that describe and compare to a given extent the available procedures for either harmonic removal, or their consideration in the identification procedure to mitigate their influence. In particular [8] proposes a classification of methods, independently of the application. Previously Manzato et al. [9,10] reviewed some methods as they apply to wind turbines, and in a recently published review paper [11], the authors analyze and classify methods to circumvent the presence of harmonics in the light of OMA methods for off-shore wind turbines. In this last paper, algorithms, combining OMA and harmonic removal techniques, are classified according to their suitability for damping estimation, taking into account nine different criteria.

From the analysis of the literature, it becomes clear that an optimal solution does not exist, since the most appropriate one is always problem driven. However, the classifications proposed in the above-mentioned papers, based on criteria such as the prior knowledge of the harmonics frequency, or on the distinction between "pre-processing techniques" and those that incorporate the harmonics into the identification method, may help to find the best choice. In this paper we will focus on on-shore wind turbines, for which we propose a novel technique that overcomes some of the main limitations found with previously published methods.

The oldest reported methods belong to the techniques denoted broadly as Time Synchronous Averaging (TSA), which are intuitively sound and easy to implement, at least in their most basic form. TSA was proposed for wind turbines in Peeters et al. [12] and has been more recently used in Manzato et al. [10]. The idea is to average consecutive cycles of the signal to eliminate its stochastic part and retain the deterministic (periodic) one; this is to say, TSA is an implementation of a so called comb filter, as shown in Braun [13]. TSA has been historically used in the domain of order tracking to obtain the harmonics shape, once the fundamental frequency is known. In the case of OMA, once the periodic signal, i.e. harmonic, is obtained, it is removed from the raw data and then the OMA method at hand is routinely applied.

The limitations of TSA become evident. First of all, the frequency of the fundamental harmonic (averaging period), must be known. If the frequency is not constant, the signal should have been sampled in the "angle domain", in such a way that the number of samples per cycle is constant. If the signal is uniformly sampled in time, then it has to be up-sampled, to generate afterwards by down-sampling a constant number of samples per cycle. The procedure must be inverted after TSA to reconstruct the identified harmonic and remove it from the raw signal. Therefore, and even though the instantaneous harmonic frequency is known (this can be the case in wind turbines), the procedure can be cumbersome to apply. Moreover, there are other effects which may affect the assumed periodicity of the signals (e.g. inharmonicity) introducing a kind of "base line", or even amplitude modulation, which make the averaging senseless.

This is the reason why this family of techniques has found limited use for the problem at hand, in favor of novel proposals, though there have been recent attempts to introduce modifications, which circumvent some limitations to make TSA usable. This recently published paper, [4], introduces two methods to correct in some way the non-repetitivity of the cycles to be averaged. The technique is demonstrated with two different gearboxes of a helicopter power turbine and a turbojet engine, but has not been tried with wind turbines. In fact, TSA methods have so far demonstrated limited success with wind turbines [14].

Another method that makes use of the angular domain sampling is the Order domain deletion (ODD) [15]. Unlike TSA, the harmonic removal is thoroughly carried out in the frequency domain, by DFT editing in the band around the harmonic frequency. The editing is performed by a linear or spline fit between the band edges. It is extremely simple when it comes to implementation, and seemingly very effective when the harmonic perturbation is highly stationary. In wind turbines, unfortunately, the harmonics are strongly time-variant in both amplitude and frequency. Moreover, the DFT editing process is highly sensitive to noise, which acts as an uncertainty on the interpolation parameters.

Let us also mention the so-called Random Decrement Technique (Randomdec), which resembles TSA in the sense that selected portions of the signal are properly averaged. It was proposed in the context of vibration signature analysis [16] and revisited in OMA [17], as a method to estimate autocorrelation functions [18,19]. More recently, it has also been proposed for harmonic removal [20] but it has only been tested on synthetic signals.

We have already mentioned that TSA analysis requires prior knowledge of the frequency of harmonics to be estimated and removed. This can be accomplished in the frequency domain from the acceleration signals if we assume that harmonics show up as isolated, narrow, spectral peaks, centered at the harmonic frequency. This is equivalent to the assumption that harmonics are those calculated, by the OMA procedure, as modes with zero damping.

Unfortunately, this is not what happens in real situations where we have a mixture of mechanical modes and harmonics with considerable frequency spread (leakage). To discriminate between harmonics and real modes, and eventually eliminate them, several procedures are proposed.

First of all, we can mention procedures based on ceptstral analysis, a classical signal processing technique, applied for the first time for OMA in Randall et al. [21]. According to this idea, harmonics become clear ceptstral peaks (called rahmonics), whereas modes show up broader. Such cepstral peaks can then be edited (removed) [22], and then the inverse transformation is applied resulting in a signal free from harmonics. This technique has also been used in Liu et al. [23], as a preprocessing step for SSI (Stochastic Subspace Identification) based OMA, but making use of synthetic data for a quarter vehicle model, with very controllable inputs. From the same authors in Randall et al. [24], in the work [25] it is shown how signal preprocessing based on cepstrum editing renders even poorer results than with TSA. Polymax algorithm was used to identify the modes.

With the same aim to distinguish between real modes and harmonics, two related procedures have been proposed. They are based on the assumption that harmonics and modes exhibit a very different behavior in terms on their statistical distribution, or PDF. According to [26], the structural response in the case of a structural mode is approximately Gaussian, whereas for an ideal harmonic is close to that of a sinusoidal signals, exhibiting high tails [8]. To asses which is the case, the raw signal must be filtered by a bank of narrow bandpass filters centered at every frequency bin, and the output evaluated to see if it corresponds to a harmonic or a mode [5].

This is a qualitative approach that can be quantified by the use of a numerical indicator such as the Kurtosis [3,5,26–28] which measures the extremities or tails of the distribution. Another alternative parameter, less used, is Entropy [29]. It is known that a Gaussian distribution has a kurtosis of 3, whereas for a pure harmonic is close to 1.5. As in the case of the PDF calculation, a bank of filters need to be used, which is a cumbersome procedure. Some recent work, and our own experience, questions the distinction of harmonics and modes on the basis of their statistical behavior for the case of wind turbines [30] where harmonics exhibit both frequency and amplitude modulation. Let us also mention the Gabor transform/expansion for order tracking [31], a well-known tool for manipulating signals in the time–frequency domain, which is equivalent to a filter bank analysis. A particular component Gabor expansion is a result of a simple spectrogram masking where the bins of interest are kept and the rest is pulled to zero. This is a filter with a sharp cutoff, whose bandwidth can be adjusted by a masking function.

Another family of methods is based on the so called Transmisibility Functions (TF) introduced in [32–34]. The original idea is to calculate ratios between different responses in the structures, in such a way that the poles of such ratios are independent of the excitation and thus the harmonics. Actually, this constitutes by itself an alternative method for OMA (denoted TOMA by the authors) making no assumptions on the excitation signal. Apart from the need to have available a number of signals (sensors), the load conditions on the wind tower must be sufficiently different to obtain the different transmissibility functions. To cope with this practical limitations the same authors have proposed a time varying version of the TOMA [35]. The technique has limited practical application, as recognized by the same authors in Daems et al. [36] mainly due to the need of a multiplicity of signals, and is difficult to automate. Other approaches include separation for blind identification [37] and periodogram ratio based harmonic removal [38].

To complete the picture, we should mention OMA methods that incorporate, in some way, an a priori knowledge of the harmonics, as known solutions, forcing that unknown solutions correspond exclusively to modes (mathematical modes may remain). Therefore, in contrast with other previously referred techniques, harmonics are not subtracted from the raw signal or “deleted” from the spectrum. There are in the literature several combinations of ways to model the harmonics (known solutions) and the OMA method, and thus is not easy to compare them or even categorize. We can mention an early work on the modification of the Least-Square Complex Exponential (LSCE) [39] identification, and by the same authors using Eigensystem Realization Algorithm (ERA) [40], which requires an exact knowledge of the poles representing the harmonics. A similar approach, but now with the Stochastic Subspace Identification (SSI) method has been proposed in Dong et al. [41] and applied to off-shore wind turbines. Gres et al. also make use of (SSI) [6,42,43], though it is not evident how the harmonics are estimated before to project them onto the raw signal before applying SSI algorithm.

A major constraint of the majority of the state-of-the-art methods described above is related to the assumption that the harmonic content is quasi-stationary, which means that their instantaneous parameters generate a negligible bandwidth around the nominal frequencies. This assumption is, however, not valid for wind turbines because persistent wind field fluctuations in the rotor plane induce constant time changes in aerodynamic loads [14,44]. These loads acting on the rotor affect the azimuth that, in turn, give rise to non-stationary instantaneous amplitude (IA) and phase (IP) in the harmonics [45]. The result is a harmonic spectral peak broadening – harmonic bandwidth increase – which can jeopardize the estimation of structural modes [8]. This is especially important for low-order harmonics (e.g. 1P – rotor rotational frequency and 3P – tower shadow effect), which possess a considerable energy and are clustered together with the first bending Fore-Aft natural frequency (FA).

If it is true that some of the referenced papers consider the possibility of frequency (or phase) variations, i.e. frequency modulation, the relevance of amplitude modulation, that significantly contributes to peak broadening in WT, has not been highlighted until recently [36]. Amplitude modulation is the main concern of this paper that do not consider simultaneous frequency modulations.

Aware of the drawbacks mentioned above, we have designed a novel approach to harmonic estimation and removal in wind turbines inspired by the techniques which appear in speech and audio signal synthesis and coding [46–49]. It turns out that audio signals bear certain similarity to vibration signals, in the sense that tonal music sounds are made out of time-variant deterministic plus stochastic contribution. For instance, in a wind instrument the deterministic sound component stems from the sustained oscillations in the resonator cavity whilst the stochastic component comes from the turbulent airflow through the instrument’s slit. Accordingly, the sustained sounds produced by musical instruments can be modeled as the sum of non-stationary sinusoids plus a residual. In the present work, the harmonic disturbances in vibration signals are conceived as a collection of time-varying harmonically related sinusoids whose instantaneous amplitude and phase change over the time record. Those variations are simultaneously captured by low-degree polynomials, whose coefficients describe the relationship between harmonic instantaneous amplitude and phase in the analysis frame. Assuming that the harmonic dynamics evolve in time around some mean fundamental frequency, we show that the proposed model is unique and computationally reduces to resolving an overdetermined linear system of equations. The minimum-norm solution yields an estimate of the harmonic polynomial coefficients, which can readily be plugged in the signal model to obtain the

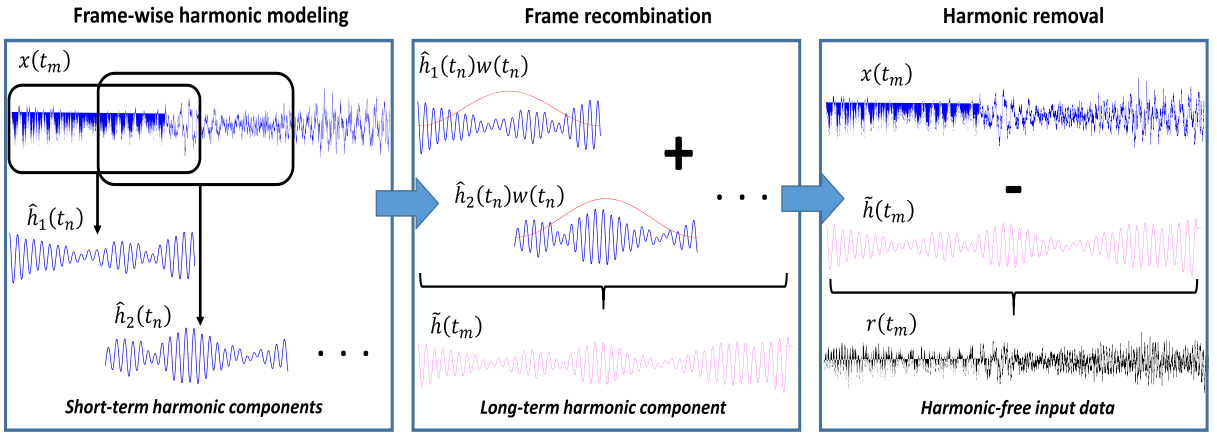

Fig. 1. Schematic pipeline of the proposed harmonic removal algorithm.

corresponding waveform. The full record harmonic disturbance is synthesized by combining neighboring analysis frames via the weighted overlap-add method (WOLA), which ensures smooth waveform transitions over the frames [50]. The final step in the proposed method consists in subtracting the estimated harmonic waveform from the input data, which is now harmonic-free and can further be analyzed by well-known OMA techniques. A schematic overview of the herein proposed method is outlined in Fig. 1.

An additional advantage of the method proposed, with respect to other approaches described above, is that the value of the instantaneous frequency does not need to be accurately known, and of course, it is not assumed constant. The algorithm actually provides an estimate of the harmonic instantaneous phase and thus frequency, which can be useful in tracking applications. In this sense, it goes further than classic schemes of harmonic (or order) tracking based for instance in Vold-Kalman filtering [51–54]. Moreover, each desired harmonic can be separately estimated, without the limitation of other approaches that estimate all orders of a given fundamental frequency.

We have conducted an algorithm performance study involving three distinct state-of-the-art methods for estimation of harmonic content in acceleration data. The reference methods were chosen to be the Local Synchronous Fitting approach [4] (from now on LSF), the second-generation Vold-Kalman Filter [51,52] (from now on VKF) and the Order Domain Deletion (from now on ODD) [15]. LSF method is an extension of the Time Synchronous Average approach (TSA) to deal with non-stationary harmonic perturbations. The algorithm core makes use of the polynomial fit over a reduced number of fundamental periods to estimate time-variant mean. As the method relies on the component period length normalization, the data needs to be resampled in the angular domain, processed and interpolated back onto the original time grid. The VKF is a classical approach to harmonic component tracking in vibration data. The problem is formulated through the structure and data equations, which are combined into a set of linear equations whose solutions are harmonic instantaneous amplitudes. The instantaneous frequency is assumed known. The filter can be formulated with different numbers of poles to alter its band-pass characteristics. An input parameter is the filter bandwidth or, interchangeably, the weighting factor, which controls filter selectivity in the frequency domain. Although there are adaptive, computationally more efficient versions of the VKF, the present study is not focused on the computational cost.

The LSF is shown to be equivalent to an LTI comb filter whose bandwidth depends on the polynomial degree and window length. In practice, it means that all the band-pass replicas are configured by two degrees of freedom. This renders the same bandwidth and selectivity for all harmonic bands, which may hamper the algorithm's discrimination performance in scenarios of structural mode – harmonic spectral overlap. The VKF can also be seen as a bank of band-pass filters, where the bandwidth can be orthogonally adjusted for each filter. This feature, which is shared by the proposed method, can be very useful in selective harmonic removal, given that some a priori knowledge about the system under test are known. In practical applications of the VKF one does not tune the noise variance: the parameters to be tuned by the user are either the variance ratio (also known as the weighting factor in the loss function) or the bandwidth. Often, it is the bandwidth that is adjusted, as this parameter is more user-friendly than the former (e.g. we usually know an approximate bandwidth for a given rotating machinery application). The relationship between those parameters is explained in the literature e.g. [52].

The ODD method, similarly to the LSF, makes use of the angular domain signal resampling in order to mitigate the effect of time-varying instantaneous rotating frequency. However, unlike the LSF and VKF, the ODD does not aim at extracting the harmonic disturbance components from the data. It rather manipulates the magnitude DFT samples in the band around the harmonic frequency, by replacing them with a linear trend or a local spline – spectrum editing. Finally, the modified DFT is transformed back in the angular domain and the resulting signal is resampled in the time domain. To improve the accuracy, the process relies on large oversampling factors (10–20).

This paper is organized as follows. In the following Section 2, we present in detail the time-variant harmonic and residual signal model for wind turbine acceleration data, together with the linear least-squares solution and its implementation for long duration registers. In Section 3, the method is validated with synthetic signals and also with signals generated by a wind turbine simulation tool. Comparisons are made against the above-mentioned methods. In section 4 we carry out a similar analysis with signals from a real

turbine. Finally, the conclusions appear in Section 5.

2. Methods

Fig. 1 outlines the chief signal processing steps in the proposed algorithm. The input single-channel acceleration data $x(t_m), m = 1,2,\cdots,M$ is split into a series of overlapped analysis frames $x_l(t_n) = x(t_n + lt_d), l = 1,2,\cdots,L$, whose processing yields the corresponding short-term harmonic components $\widehat{h}_l(t_n), n = 1,2,\cdots,N$. Next, those components are windowed by $w(t_n)$ and merged by means of the WOLA method to obtain the long-term harmonic component $\widetilde{h}(t_m)$. In the last step, the estimated harmonic perturbation is subtracted from the input and the residue $r(t_m)$ is harmonic-free.

2.1. Short-term harmonic signal modeling

Structural analysis of wind turbines is based on acceleration registers taken at different tower heights, when available, or at the nacelle, under natural excitation conditions. One such register can be modeled in a length-N analysis frame [48,49]:

$$x(t_n) = h(t_n) + r(t_n) = \sum_{k=1}^{K} A_k(t_n) cos\left(2\pi k f_0 t_n + \varphi_k(t_n)\right) + r(t_n), n = 1,2,\cdots,N. \tag{1}$$

The harmonic component $h(t_n)$ has its origin in the rotating behavior of the structure, remarkably the tower shadow effect (3P). It is therefore represented by a set of K harmonically related sinusoids with instantaneous amplitudes $A_k(t_n)$ and phases $2\pi k f_0 t_n + \varphi_k(t_n)$, being f_0 the average fundamental frequency which is usually known (e.g. a rotary encoder) and $\varphi_k(t_n)$ the non-linear instantaneous phase deviation which can also accommodate errors in the initial estimation of f_0. The residue $r(t_n)$ is stochastic in nature and contains the contribution from the structural modes and noise. The model (1) cannot be uniquely identified because analytically, it represents a non-linear underdetermined system of equations. In order to relax the non-linearity constraint we rewrite (1) as a combination of the in-phase and quadrature terms:

$$x(t_n) = \sum_{k=1}^{K} \left(p_k(t_n) sin(2\pi k f_0 t_n) + q_k(t_n) cos(2\pi k f_0 t_n)\right) + r(t_n) \tag{2}$$

$$p_k(t_n) = -A_k(t_n) sin(\varphi_k(t_n)),\ q_k(t_n) = A_k(t_n) cos(\varphi_k(t_n)) \tag{3}$$

The system (2) is now linear-in-parameters but it still has more unknowns than equations. Let us assume that both $p_k(t_n)$ and $q_k(t_n)$ are in origin continuous functions of time. Accordingly, the products (3) are also continuous and can therefore be approximated in the analysis window by low-degree polynomials:

$$p_k(t_n) \approx p_{k,0} + p_{k,1} t_n + \cdots + p_{k,D} t_n^D,\ q_k(t_n) \approx q_{k,0} + q_{k,1} t_n + \cdots + q_{k,D} t_n^D \tag{4}$$

Combining the D-degree polynomials (3)–(4) with (2) we obtain the signal model for the input data:

$$x(t_n) = \sum_{k=1}^{K} \left(\sum_{i=0}^{D} p_{k,i} t_n^i sin(2\pi k f_0 t_n) + \sum_{i=0}^{D} q_{k,i} t_n^i cos(2\pi k f_0 t_n) \right) + r(t_n). \tag{5}$$

The last expression is next rewritten in the computationally more convenient matrix form:

$$\boldsymbol{x} = \boldsymbol{B}\boldsymbol{\theta} + \boldsymbol{r} \tag{6}$$

Vectors $\boldsymbol{x} \in \mathbb{R}^N$ and $\boldsymbol{r} \in \mathbb{R}^N$ contain the observations and noise samples respectively whilst the model parameters are stored in a vector

$$\boldsymbol{\theta} = \left(p_{1,0} p_{1,1} \cdots p_{1,D} q_{1,0} q_{1,1} \cdots q_{1,D} \cdots p_{K,1} \cdots p_{K,D} q_{K,1} \cdots q_{K,D}\right)^T \in \mathbb{R}^{K(2D+2)}$$

with $(\bullet)^T$ being the transpose operator. The regression matrix $\boldsymbol{B}$ is a block matrix whose structure is given as:

$$B = (B_1 \ \ B_2 \ \ \ldots \ B_K) \in R^{N \times K(2D+2)} \tag{7}$$

$$\boldsymbol{B}_k = (\boldsymbol{\alpha}_k \boldsymbol{\beta}_k) \times \begin{pmatrix} \boldsymbol{Z} & 0 \\ 0 & \boldsymbol{Z} \end{pmatrix} \in \mathbb{R}^{N \times (2D+2)} \tag{8}$$

$$\boldsymbol{\alpha}_k = diag([sin(2\pi k f_o t_1) sin(2\pi k f_o t_2) \cdots sin(2\pi k f_o t_N)]) \in \mathbb{R}^{N \times N} \tag{9}$$

$$\boldsymbol{\beta}_k = diag([cos(2\pi k f_o t_1) cos(2\pi k f_o t_2) \cdots cos(2\pi k f_o t_N)]) \in \mathbb{R}^{N \times N} \tag{10}$$

with $\boldsymbol{Z} \in \mathbb{R}^{N \times D+1}$ being the time Vandermonde matrix:

$$\boldsymbol{Z} = \begin{bmatrix} 1 & \cdots & t_1^D \\ \vdots & \ddots & \vdots \\ 1 & \cdots & t_N^D \end{bmatrix}$$

The estimation of the parameters $\boldsymbol{\theta}$ reduces to minimizing the following cost function:

$$\widehat{\boldsymbol{\theta}} = \underset{\boldsymbol{\theta}}{argmin} \|\boldsymbol{x} - \boldsymbol{B}\boldsymbol{\theta}\|_2^2 = \left(\boldsymbol{B}^T\boldsymbol{B}\right)^{-1}\boldsymbol{B}^T\boldsymbol{x} = \boldsymbol{B}^+\boldsymbol{x} \tag{11}$$

where $(\bullet)^+$ designates the pseudoinverse of a matrix. A straightforward combination of the solution in (11) with (6) – (10) yields the estimate of the harmonic component in the analysis frame

$$\widehat{h}(t_n) = \sum_{k=1}^{K}\left(\sum_{i=0}^{D}\widehat{p}_{k,i}t_n^i sin(2\pi k f_0 t_n) + \sum_{i=0}^{D}\widehat{q}_{k,i}t_n^i cos(2\pi k f_0 t_n)\right), n = 1, 2, \cdots, N. \tag{12}$$

In addition, we estimate the instantaneous amplitude and phase deviation for each harmonic in the analysis window:

$$\widehat{A}_k(t_n) = \sqrt{\left(\sum_{i=0}^{D}\widehat{p}_{k,i}t_n^i\right)^2 + \left(\sum_{i=0}^{D}\widehat{q}_{k,i}t_n^i\right)^2} \tag{13}$$

$$\widehat{\varphi}_k(t_n) = -atan\left(\frac{\sum_{i=0}^{D}\widehat{p}_{k,i}t_n^i}{\sum_{i=0}^{D}\widehat{q}_{k,i}t_n^i}\right), k = 1, 2, \cdots, K. \tag{14}$$

Expressions (13) and (14) will be useful for calculating the harmonic bandwidth as part of the stochastic synthesis.

2.2. Long-term harmonic synthesis

Let us suppose that we have acquired from the response analogue signal a total of M samples at the time instants $t_1, t_2, \cdots, t_M = M/f_s$, $M \gg N$, with f_s being the sampling rate. A vector $\in \mathbb{R}^M$, which contain the aforementioned samples, is segmented in L overlapped analysis frames $x_l(t_n) = x(t_n + lt_d), l = 1, 2, \cdots, L$ where t_d is the time delay between contiguous frames whilst L is the number of frames covering the total duration of the input data. A successive application of the above algorithm to the overlapped analysis frames $x_l(t_n)$ (Fig. 1, left panel) generate a set of short-term harmonic segments $\widehat{h}_l(t_m - lt_d), l = 1, 2, \cdots, L$. The synthesis of the long-term harmonic waveform is carried out by means of the weighted overlap-add technique [50], which consists in the following steps (Fig. 1, central panel):

1) Each segment $\widehat{h}_l(t_m - lt_d)$ is scaled by an analysis window $w(t_n)$, whose role is to mitigate potential discontinuities at the boundaries of adjacent analysis frames. The typical choice is a raised-cosine window e.g. Hann, which possesses a convenient scaling property:

$$\sum_{l\in\mathbb{Z}} w\left(t_m - l\frac{N}{2f_s}\right) = 1$$

2) The windowed segments are linearly combined with an appropriate weighting, which compensates the windowing effect. The resulting waveform is the estimate of the harmonic disturbances in the data whose length covers M samples:

$$\widetilde{h}(t_m) = \frac{\sum_{l=1}^{L} w(t_n)\widehat{h}_l(t_m - lt_d)}{\sum_{l=1}^{L} w(t_m - lt_d)}, m = 1, 2, \cdots M \tag{15}$$

By combining (13) – (15), we also obtain the harmonic instantaneous amplitude and phase deviation for the duration of the input data:

$$\widetilde{A}_k(t_m) = \frac{\sum_{l=1}^{L} w(t_n)\widehat{A}_l(t_m - lt_d)}{\sum_{l=1}^{L} w(t_m - lt_d)} \tag{16}$$

$$\widetilde{\varphi}_k(t_m) = \frac{\sum_{l=1}^{L} w(t_n)\widehat{\varphi}_l(t_m - lt_d)}{\sum_{l=1}^{L} w(t_m - lt_d)} \tag{17}$$

Finally, by subtracting the estimated harmonic contribution from the input data we obtain the residue, which contains the natural frequencies:

$$r(t_m) = x(t_m) - \widetilde{h}(t_m), m = 1, 2, \cdots, M. \tag{18}$$

2.3. Model tuning

For the sake of implementation of the proposed harmonic signal model, we need to adjust the following analysis parameters: the number of harmonics K, the polynomial degree D and the analysis frame duration Nt_s. The number of harmonics will utterly depend on the application. For instance, in the context of the present application, both 1P component and the 3P harmonic series can potentially shadow the structural modes. Accordingly, in the harmonic signal model (5) the corresponding terms in the sum ($k = 1, 3, 6, 9$, etc.) should be considered. In other circumstances, we may need to monitor the dynamics of the tower's first bending mode, so that it is not coupled to the 1P component. In that case, the harmonic signal model would contemplate a single term corresponding to the fundamental rotational component ($k = 1$).

The polynomial degree and analysis frame time duration determine the goodness-of-fit of the model to the data in the given bandwidth around the harmonic frequencies. They act in a mutually correlated fashion in order to constrain the model to the specific bandwidth and avoid possible undesirable effects of under and overfitting. Given the polynomial degree, shorter analysis frame yields small modeling bias but can inflate variances of the estimated parameters - overfitting. Conversely, enlarging the analysis frame duration, the uncertainty of the estimates reduces and modeling bias gets larger - underfitting. Moreover, we want to keep the polynomial degree as low as possible (the parsimony principle) in order to avoid numerical instabilities when evaluating the Moore-Penrose pseudoinverse matrix in (11).

Bearing in mind the above argumentation, let us first discuss on the choice of the analysis frame duration for the problem at hand. The minimum frame duration is clearly conditioned on the mean period of the fundamental harmonic (1P or 3P as the case may be). As the signal model (5) represents sinusoids whose energy is clustered around the harmonic frequencies, the analysis frame must cover at least one period of 1P; otherwise, the fundamental component would become a trend, thus invalidating the harmonicity assumption (recall that a trend can be seen as a sinusoid whose period is larger than a given time register). In the context of the present application, we adjust the number of observations N in the way that the analysis frame covers approximately-two 1P periods: $N = 2f_s/f_0$.

As for the polynomial degree, we will assume that the instantaneous amplitude and phase deviation evolve linearly in the analysis frame. Accordingly, the expressions (3) become:

$$p_k(t_n) = -\left(A_{k,0} + A_{k,1}t_n\right)sin\left(\varphi_{k,0} + \varphi_{k,1}t_n\right) \tag{19.a}$$

$$q_k(t_n) = \left(A_{k,0} + A_{k,1}t_n\right)cos\left(\varphi_{k,0} + \varphi_{k,1}t_n\right) \tag{19.b}$$

Applying the sum-of-angles trigonometric identities to the last expressions and making use of the small argument Taylor series approximation ($sin\left(\varphi_{k,1}t_n\right) \approx \varphi_{k,1}t_n, cos\left(\varphi_{k,1}t_n\right) \approx 1$), we have:

$$p_k(t_n) \cong -A_{k,0}sin\left(\varphi_{k,0}\right) - \left(A_{k,0}\varphi_{k,1}cos\varphi_{k,0} + A_{k,1}sin\varphi_{k,0}\right)t_n - \left(A_{k,1}\varphi_{k,1}cos\varphi_{k,0}\right)t_n^2 =$$

$$= p_{k,0} + p_{k,1}t_n + p_{k,2}t_n^2 \tag{20.a}$$

$$q_k(t_n) \cong A_{k,0}cos\left(\varphi_{k,0}\right) - \left(A_{k,0}\varphi_{k,1}sin\varphi_{k,0} - A_{k,1}cos\varphi_{k,0}\right)t_n - \left(A_{k,1}\varphi_{k,1}sin\varphi_{k,0}\right)t_n^2 =$$

$$= q_{k,0} + q_{k,1}t_n + q_{k,2}t_n^2 \tag{20.b}$$

Subsequently, we choose the second-degree polynomials for the estimation of the harmonic model (5). Observe in (20.a) and (20.b) that the parameters $p_i, q_i, i = 0, 1, 2$ possess certain internal structure, which depend on $\left(A_{k,0}, A_{k,1}, \varphi_{k,0}, \varphi_{k,1}\right)$. Albeit this information might enclose certain relationships between the instantaneous amplitude and phase deviation, it will not be dealt with in the present work. In the next section, we show that this choice for the polynomial degree and analysis frame duration is well suited to real wind turbine signals.

2.4. Stochastic synthesis

By subtracting the estimated long-term harmonic component from the input data, we obtain a residue that contains the structural modes and background noise. The harmonic removal, however, generates dips in the residual power spectrum around the harmonic frequencies. This stems from the fact that we do not assume an a priori knowledge on the noise power spectral distribution; consequently, we ignore the mixing between the harmonics and noise. Accordingly, we treat the noise in a non-parametric way and thus allow the harmonic model to be locally contaminated i.e. the harmonic bandwidth contains some small fraction of noise as well.

In order to compensate this effect, for each harmonic we generate a narrow-band noise centered at the harmonic average frequency and delimited by the harmonic bandwidth. From the time–frequency analysis theory, we know that this parameter can be readily calculated as in [55]:

$$BW_k^2 = BW_{k,A}^2 + BW_{k,\varphi}^2 = \frac{1}{f_s}\sum_{m=1}^{M}\left(\widetilde{A}_k'(t_m)\right)^2 + \frac{1}{f_s}\sum_{m=1}^{M}\left(\widetilde{\varphi}_k'(t_m) - 2\pi f_0\right)^2\left(\widetilde{A}_k(t_m)\right)^2 \tag{21}$$

In the last expression, $BW_{k,A}^2$ and $BW_{k,\varphi}^2$ are the instantaneous amplitude and phase contributions to the harmonic bandwidth respectively. The operator $(')$ is the first time derivative whereas $\widetilde{A}_k(t_m)$ and $\widetilde{\varphi}_k(t_m)$ are calculated as in (16) and (17). Although the

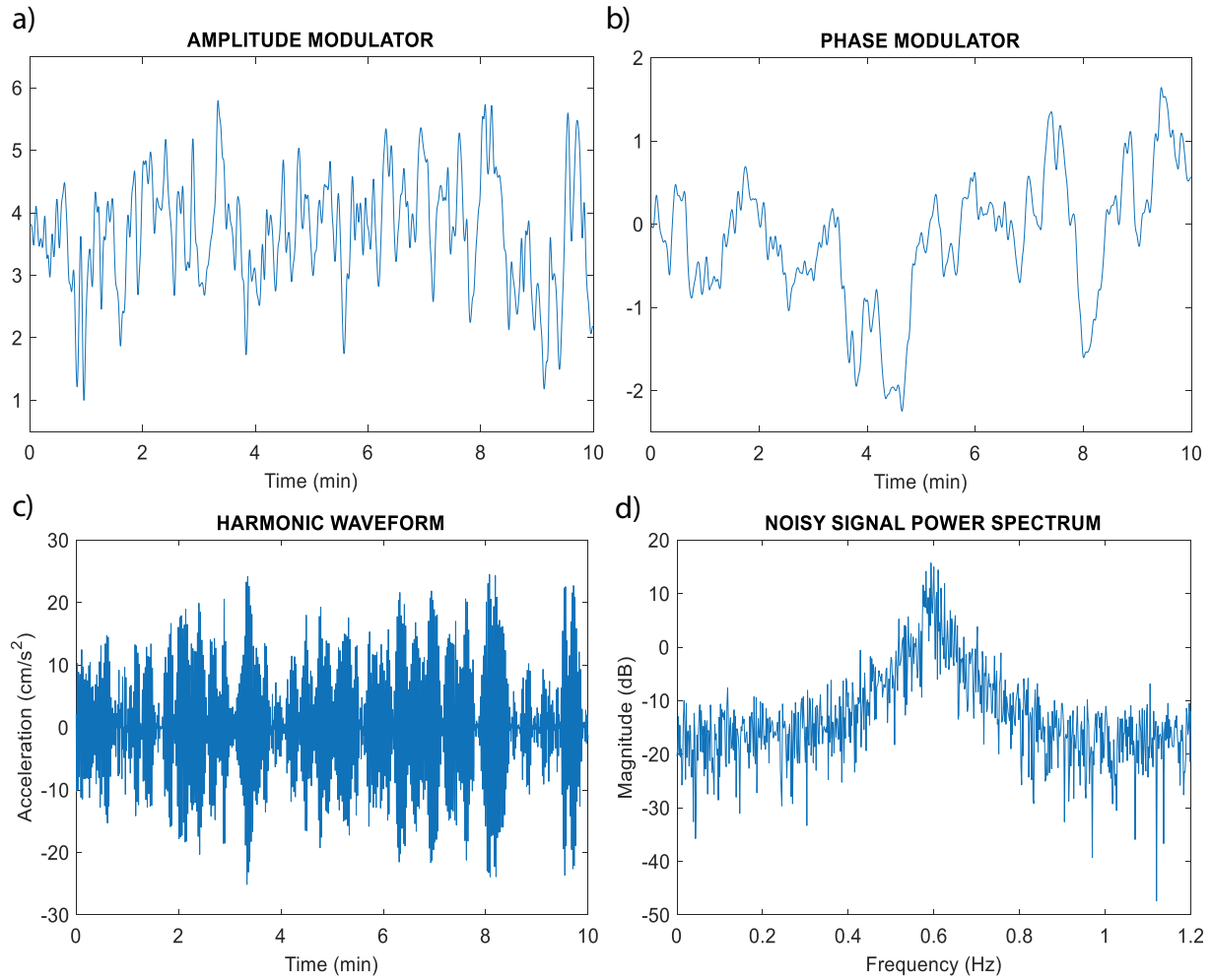

Fig. 2. A single realization of the AMPM harmonic sinusoid defined in (22).

current stochastic synthesis step successfully reconstructs the wind turbine power spectrum around the harmonic perturbations, it is not essential for the correct operation of the proposed harmonic removal algorithm and can thus be omitted. For this reason, it is not part of the algorithm general scheme in Fig. 1.

3. Results: Synthetic data

We have carried out a number of studies, concerning both synthetic and real data, in order to assess the performance of the proposed algorithm. First, we present a sensitivity analysis of the input parameters – frame size and polynomial degree. Next, we describe a comparative study, which involves three reference state-of-the-art methods and a number of representative analysis scenarios regarding the present application. In section 4, we will complement this analysis with the discussion of three illustrative real-world case studies.

3.1. Input parameters sensitivity

The aim of the present sensitivity study is to evaluate the goodness-of-fit of the proposed method as a function of the input parameters i.e. how well the method can capture the non-stationarities in a harmonic component given the frame size and polynomial order. To that end, we made use of synthetic data for simulating non-stationary harmonics in presence of a stochastic perturbation. A harmonic is conceived as a carrier sinusoid, jointly modulated in amplitude and phase (AMPM):

$$H_e(t_n) = H(t_n) + e(t_n) = (1 + \mu_a a(t_n))sin(2\pi f_0 t_n + \mu_\varphi \varphi(t_n)) + e(t_n) \tag{22}$$

where $a(t_n)$ and $\varphi(t_n)$ are the amplitude and phase modulator respectively, μ_a and μ_φ are the modulation indices whilst f_0 is the carrier

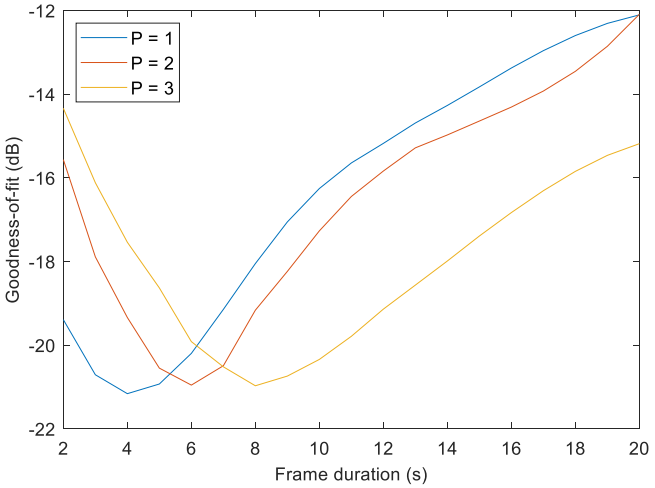

Fig. 3. Goodness-of-fit for the single harmonic as a function of the input parameters.

frequency and $e(t_n)$ the normally distributed measurement noise. The modulators are generated as an output of an autoregressive process AR(1) defined as:

$$a(t_n) = \beta_a a(t_{n-1}) + \gamma(t_{n-1}), \gamma \propto \mathcal{N}\left(0, \sigma_\gamma^2\right)$$

$$\varphi(t_n) = \beta_\varphi \varphi(t_{n-1}) + \delta(t_{n-1}), \delta \propto \mathcal{N}\left(0, \sigma_\delta^2\right)$$

$$\beta_a = \frac{r_{a,0} - \varepsilon_a}{r_{a,0}}, \sigma_\gamma^2 = r_{a,0} - \beta_a\left(r_{a,0} - \varepsilon_a\right),$$

$$\beta_\varphi = \frac{r_{\varphi,0} - \varepsilon_\varphi}{r_{\varphi,0}}, \sigma_\delta^2 = r_{\varphi,0} - \beta_\varphi\left(r_{\varphi,0} - \varepsilon_\varphi\right).$$

The autoregressive model parameters were set as $r_{a,0} = r_{\varphi,0} = 1$, $\varepsilon_a = 5 \times 10^{-3}$, $\varepsilon_\varphi = 10^{-3}$; the settings for the model in (22) were $\mu_a = 0.75, \mu_\varphi = 2, f_0 = 0.6Hz$ and the measurement noise variance equal to 1.5. The modulators are further smoothed out by an order-3 Butterworth filter of cutoff frequency equal to 0.2 Hz. An illustration of a single realization of (22) is shown in Fig. 2.

The goodness-of-fit (GOF) of the proposed model to the data was defined as the Residue-to-Harmonic ratio:

$$GOF_{dB} = 10log_{10}\frac{\sum_n (H(t_n) - \widehat{H}(t_n))^2}{\sum_n H^2(t_n)}$$

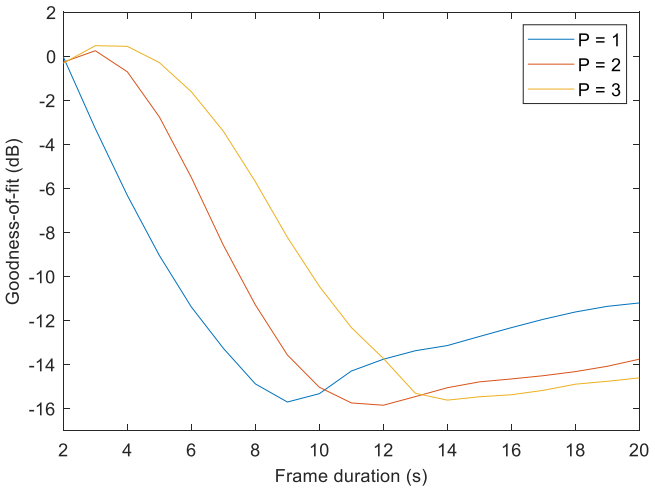

Fig. 4. Goodness-of-fit for the mode-harmonic mixture as a function of the input parameters.

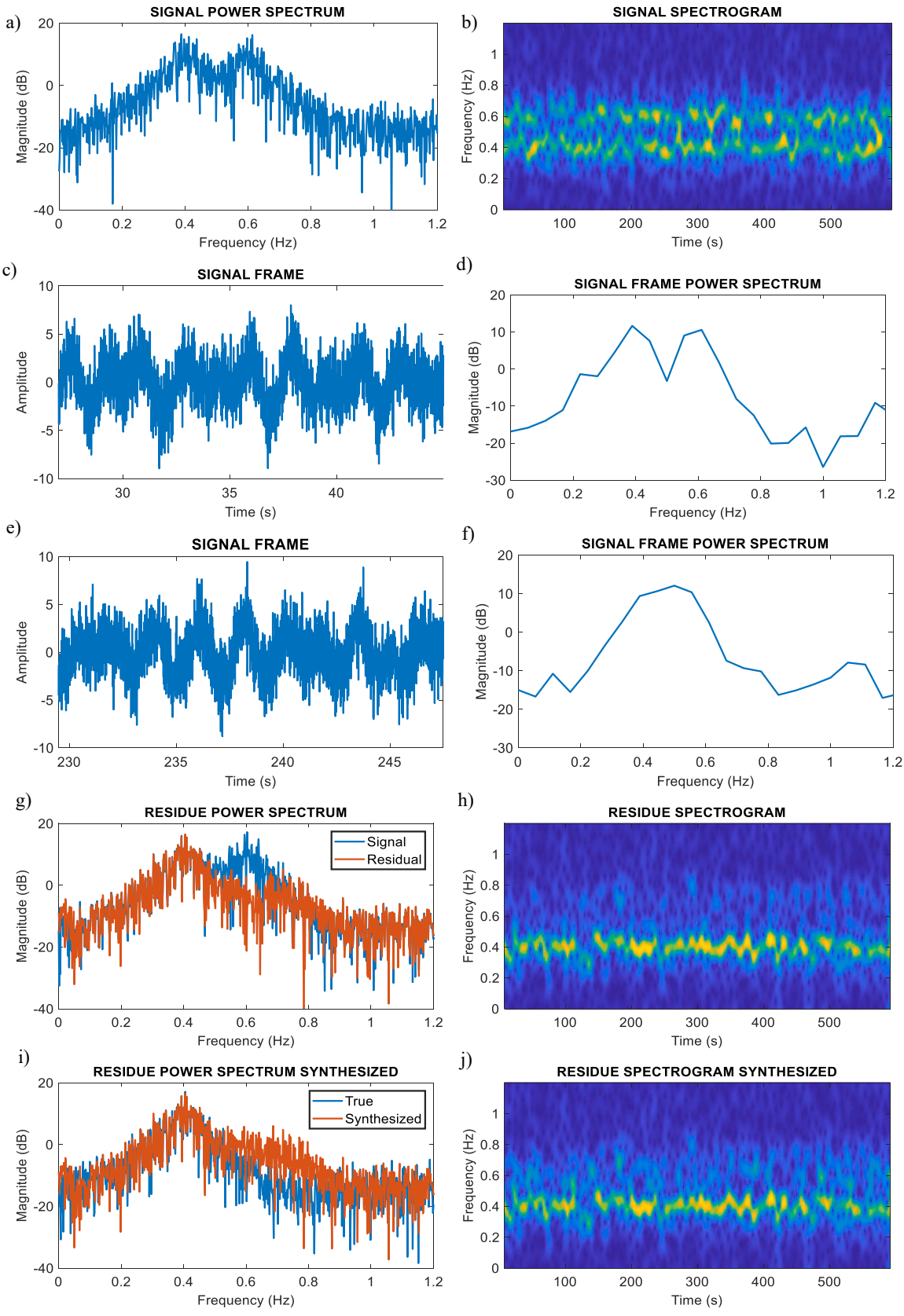

(caption on next page)

Fig. 5. Illustration of the mode-harmonic collision scenario analysis/synthesis.

Table 1
NREL 5 MW wind turbine principal vibration mode characteristics.

Vibration mode	Natural frequency (Hz)	Damping (%)
Fore-aft 1 (1st FA)	0.33	8.1
Fore-aft 2 (2nd FA)	2.89	1.9

Table 2
Synthetic data wind speed – 3P frequency relationship.

Wind speed (m/s)	3P frequency mean ± standard deviation (Hz)
8	0.452 ± 0.055
10	0.534 ± 0.060
12	0.596 ± 0.019
20	0.604 ± 0.026

Table 3
Input parameter values for the comparative study.

Wind speed	LSF		VKF		ODD		Proposed	
	Order	Window length (3P cycles)	Order	Bandwidth (Hz)	Interpolation	Bandwidth (Hz)	Order	Window length (1P cycles)
8 m/s	3	7	2	0.12	linear	0.12	1	2
10 m/s	3	7	2	0.21	linear	0.21	1	2
12 m/s	3	5	2	0.26	linear	0.26	2	2
20 m/s	3	5	2	0.30	linear	0.30	2	2

where $\widehat{H}(t_n)$ is the estimated harmonic waveform. For each combination of frame duration (ranging from 2 s to 20 s) and polynomial degree (ranging from 1 to 3) 100 realizations of (22) were performed and the mean GOF was calculated. The overall results for a single harmonic are shown in Fig. 3. The curves corresponding to different polynomial degree (P) exhibit a similar general trend, comprising global minima, which indicate the most optimal working point in the sense of mean square error. The minima shift towards larger frame durations as P increases, because the model flexibility grows as well. The curve segment to the left of a minimum designates an underfit, whilst the segment to the right specifies an overfit. Working with $P = 1$ allows for a short frame duration; however, its relatively sharp minimum can easily drive the analysis into the over/underfit zone. Larger P yields broader minima and accordingly an extended flexibility in choosing the frame duration. The aforementioned discussion is immediately extended to a set of harmonics simultaneously present in the data.

In the context of the present application, we often encounter the situation of a partial collision (overlap) between a vibration mode and a harmonic. Such scenarios typically comprehend the interaction between the 1st FA and 3P component, as well as between the 2nd FA and a higher order harmonic. Under these circumstances, the above analysis needs to be reexamined because harmonic removal could seriously corrupt the vibration mode content and consequently hamper its identification. Therefore, we seek to estimate the harmonics and simultaneously preserve the modal content as much as possible. As for the synthetic signal, we have considered the following:

$$H_e(t_n) = M(t_n) + H(t_n) + e(t_n) = \sum_{k=1}^{2} \left(1 + \mu_{a,k} a_k(t_n)\right) sin\left(2\pi f_{0,k} t_n + \mu_{\varphi,k} \varphi_k(t_n)\right) + e(t_n) \tag{23}$$

In the last expression, the mode $M(t_n)$ and the harmonic $H(t_n)$ share the same model, whilst the carrier frequencies are $f_{0,1} = 0.4Hz$ and $f_{0,2} = 0.6Hz$ respectively. We believe that this assumption is valid because a vibration mode driven by a stochastic enforcement manifests itself in the signal domain as a modulated sinusoid. The GOF for the current model was defined with respect to the vibration mode:

$$GOF_{dB} = 10log_{10} \frac{\sum_n \left(M(t_n) + H(t_n) - \widehat{H}(t_n)\right)^2}{\sum_n M^2(t_n)}.$$

The same analysis was performed as in the single harmonic study, and the results are shown in Fig. 4. The global minima in the curves, which quantify the algorithm's discrimination capacity, correspond to larger frame duration values when compared to the results in Fig. 3. This is equivalent to restricting the model flexibility in order to avoid hampering the information from the vibration mode. It turns out that such a situation is quite common in wind turbine acceleration signals and will be taken into account in the following studies.

An example of the present harmonic extraction scenario is illustrated in Fig. 5, where the analysis and synthesis algorithm steps are shown in both frequency and time–frequency domain. The input signal power spectrum and its spectrogram appear in a) and b) respectively. By a visual inspection of the local maxima position in the spectrogram one might judge that the components do not

overlap in frequency and that they are fully resolved. This is, however, far from true and to this end, we illustrate the overlap effect on two signal segments localized at 36 s and 238 s with respect to the full segment duration. In c) and d) the components are indeed resolved in the frequency domain. However, in e) and f) the components strongly overlap, in the way that they merge into a single spectrum peak. These examples show that the non-stationarity in amplitude and phase can create very different analysis scenarios across the analysis frames, producing the time-varying harmonic bandwidth.

The effect of harmonic removal on the residue is shown in g) and h). For the sake of clarity, the power spectrum of the residue is plotted on top of the original power spectrum. Inlet i) shows the synthesized power spectrum of the residue by means of (21), together with the mode power spectrum. Finally, the synthesized residue spectrogram is shown in (j).

3.2. Performance comparative study on synthetic wind turbine data

As we are dealing with an application in the context of wind energy, the current study has been carried out using the OpenFAST software [56]. This is a free and open software developed by NREL (National Renewable Energy Laboratory) that is certified for the design of on-shore and off-shore wind turbines. This software is a standard for the design of components and aerodynamic, aeroelastic, structural and control system simulations. It allows highly realistic simulations under different wind turbine operating conditions. It is able to determine the position, velocity and acceleration of several points of the machine as well as the structural loads applied to its components.

OpenFAST models a wind turbine with 24 degrees of freedom (DOFs): 6 DOFs for the base/cementation movement, another 4 DOFs to describe the tower flexibility (2 lateral and 2 longitudinal), 1 DOF representing the nacelle yaw, 1 DOF for the generator rotation and 1 more for the drive-train flexibility. In turn, each blade is modeled by means of 3 DOFs, 2 flapwise and 1 edgewise mode. The last 2 DOFs consider the rotor- and tail-furl motion. The model allows specifying the structural properties (stiffness, damping, inertias) of tower, drive-train and blades, as well as the geometrical and aerodynamic properties of tower and blades. In addition, it allows the placement of virtual sensors (accelerometers, IMU-s and strain sensors) at arbitrary locations of tower, drive-train and blades. This allows obtaining information of these variables in simulation for off-line post-processing.

The 5 MW on-shore wind turbine simulated in this work consists of a 3-bladed, 126 m diameter wind rotor on a tower 87.6 m high.

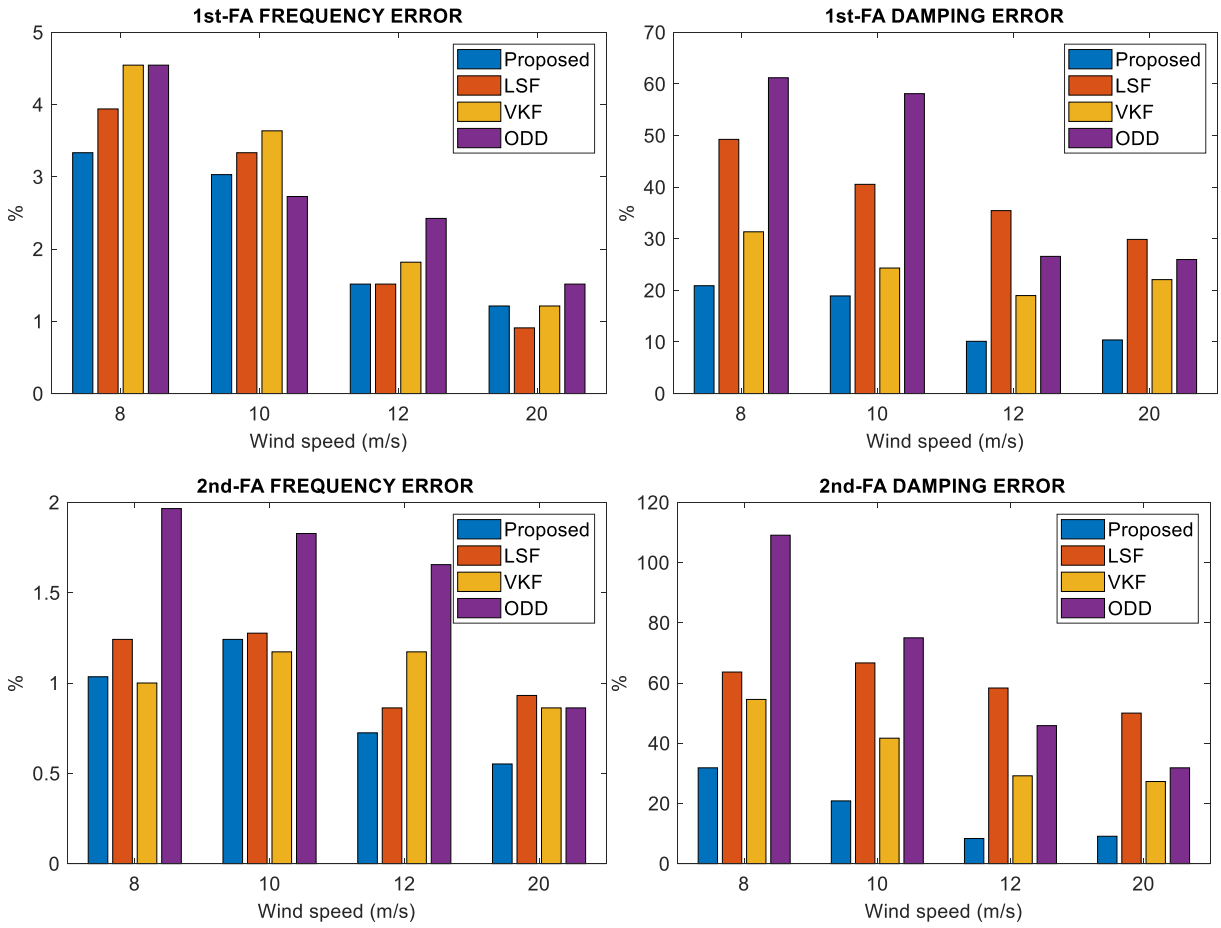

Fig. 6. Comparative study results in terms of relative error.

This wind turbine model has also been developed by NREL, and has widely been used in a plethora of research projects. For the most salient properties of the turbine, the reader is referred to [57].

The characterization of the principal vibration modes (1st FA and 2nd FA) in terms of natural frequency and damping is to be found elsewhere in the literature [58,59]. In Bir et al. [58], these values are calculated making an eigenanalysis of the azimuthally-averaged linearized system after applying the Multi-Blade Coordinate (MBC) transformation. Due to internal and external anisotropies, the MBC transformation does not produce an exact Linear Time-Invariant (LTI) system, and a Floquet analysis is required to capture the influence of all periodic terms, leading to a more accurate stability analysis [59]. In both cases, the simulations have been performed using deterministic winds, while the simulations performed in this paper have been carried out with turbulent winds, so small differences in the values of frequencies and modal damping obtained are to be expected. The mode characteristics used for the present study are shown in Table 1.

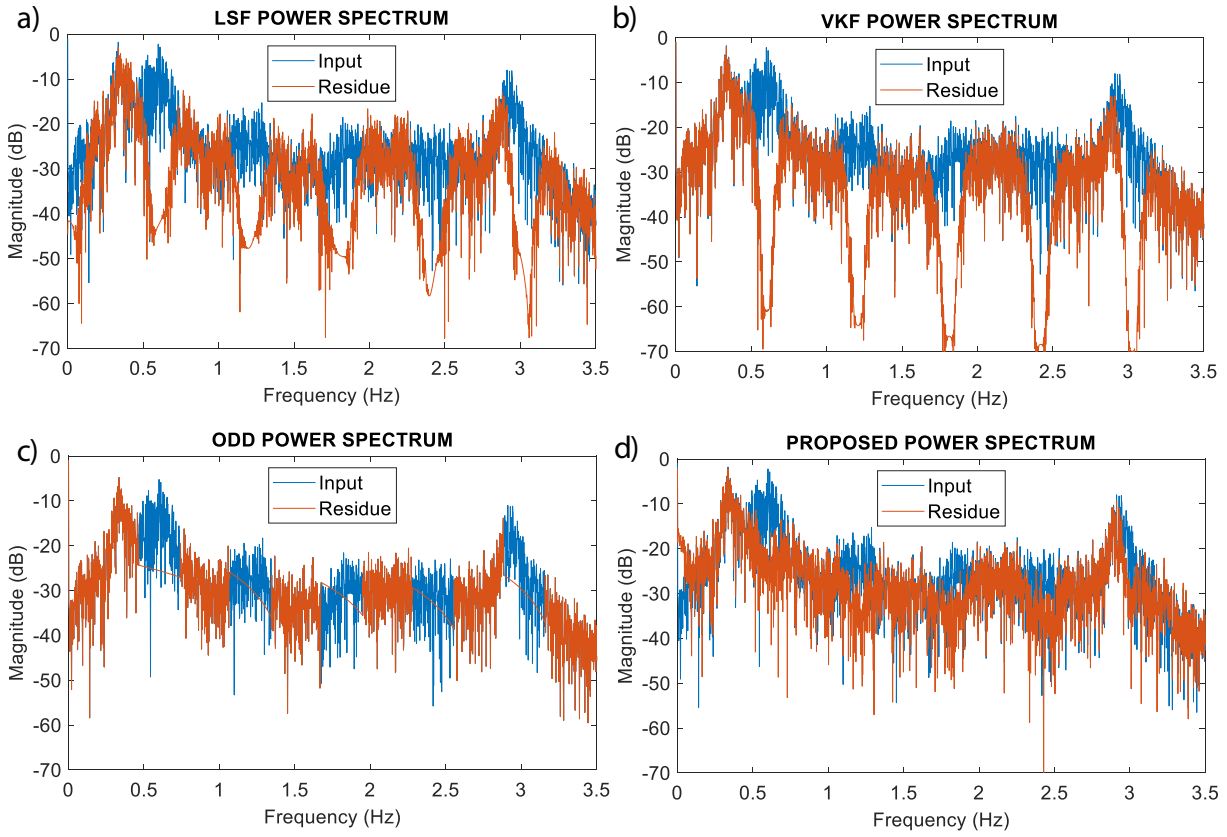

Fig. 7. Harmonic removal by the benchmark methods for wind speed of 20 m/s.

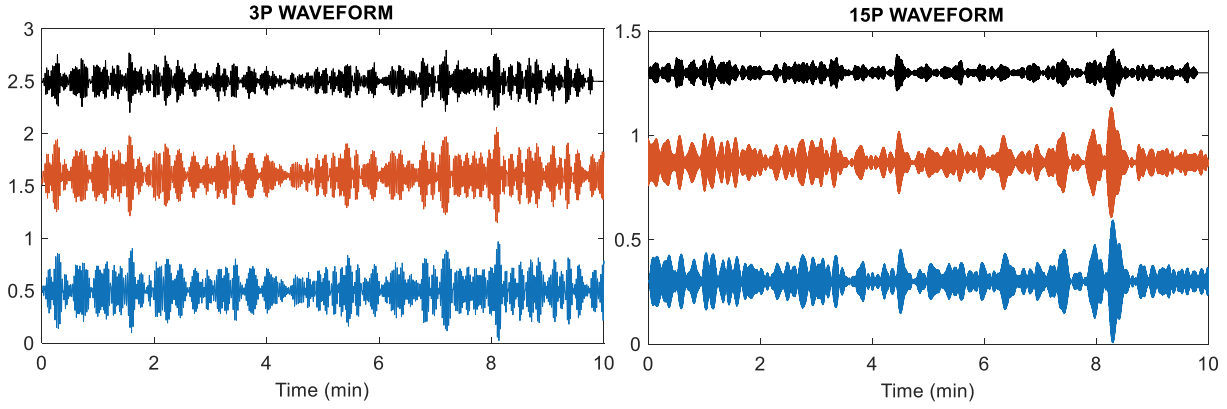

Fig. 8. Estimated harmonic 3P and 15P waveforms by the LSF (blue), VKF (red) and proposed (black) for wind speed of 20 m/s. (For interpretation of the references to colour in this figure legend, the reader is referred to the web version of this article.)

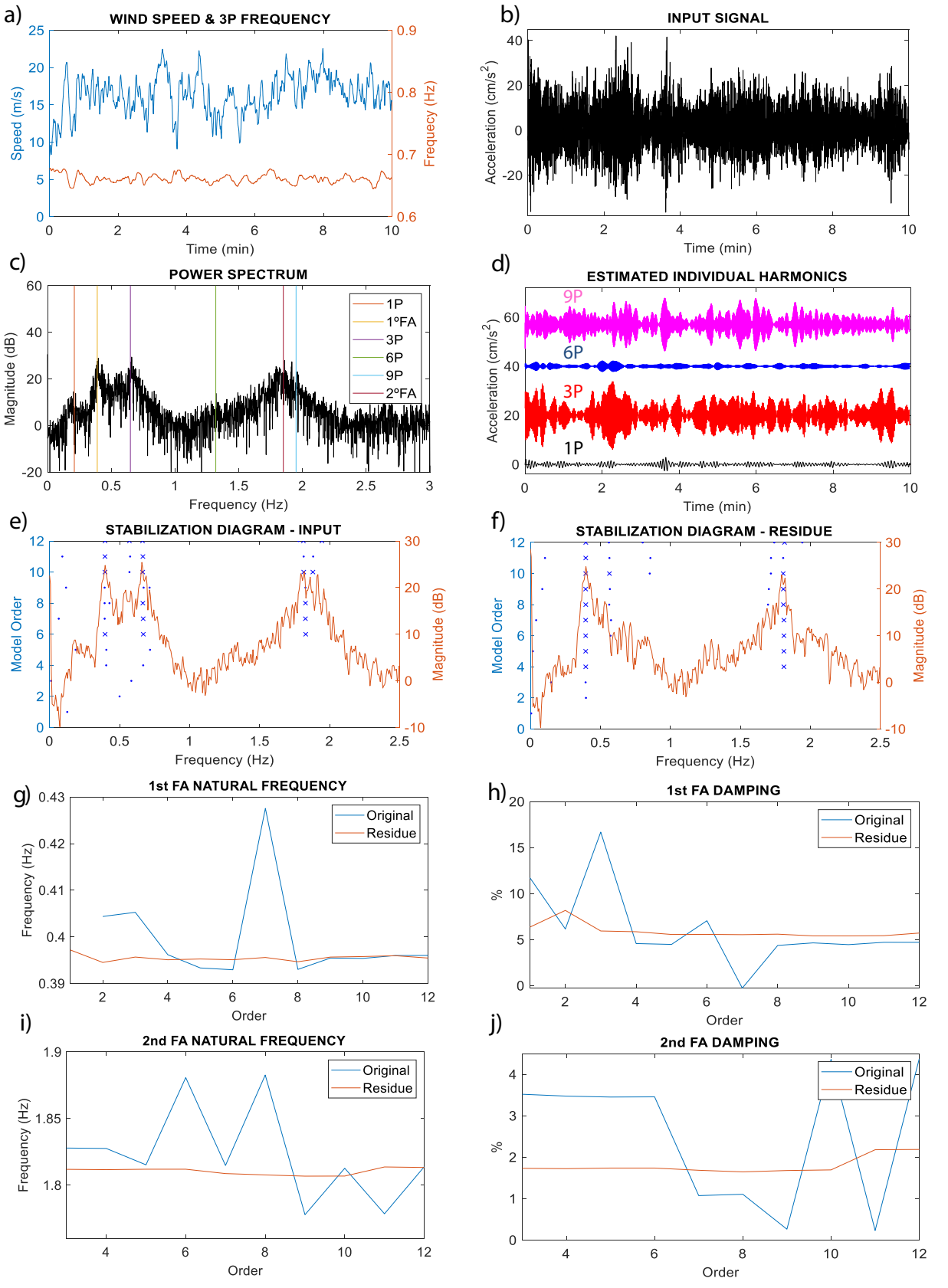

(caption on next page)

Fig. 9. Case study 1 - Quasi-uniform high-speed wind with considerable amount of turbulence. The frame length is 9 s and polynomial order equal to 2.

We have generated a number of synthetic 10-minute acceleration data records in such a way to cover scenarios of both low and high-speed wind, which in turn produce a variety of interactions between the vibration modes and harmonics. The relationship wind speed – 3P frequency for the data is shown in Table 2. Observe that low wind speed scenarios produce two undesired effects: 1) the 3P component is moved closer to the 1st FA, 2) the 3P standard deviation gets larger. As a consequence, the overlap between the 1st FA and 3P grows bigger, which seriously hampers harmonic removal. Similar argumentation can be brought out for the 2nd FA and the surrounding high-order 3P harmonics.

In the present study, our aim was to emulate a scenario, which becomes more and more frequent in in OMA-related applications. Instead of performing the full structural analysis off-line, the current trends in structural health monitoring point towards in-situ signal processing by a stand-alone low-cost sensor. The fact that some calculations are performed on-line allows for a larger time margin for maintenance-related mechanisms. The downside to this is that only few, if any, SCADA information channels are available, which often means that there is no access to the instantaneous tachometer output. Accordingly, the data input to the benchmark methods is the fore-aft acceleration and average rotational speed over 10 min registers.

In order to establish a fair comparison, we ensured that the input parameters of the methods were adjusted optimally in the context of the present application. Regarding input frequency information, the 3P mean was fed to all the methods. As for the additional input parameters, we proceeded as follows. In the LSF, the filter order was set to 3 for all the data (as recommended in Abboud et al. [4]), whilst the window length was signal customized in order to set the lower cutoff 3P bandwidth at the arithmetic average between the 1st FA and 3P mean frequency. For the VKF the filter order was equal to two; as for the bandwidth, the same criterion as for the LSF was applied. The ODD also used the same bandwidth criterion, whilst the interpolation mode was linear in all the cases. In the proposed method, the frame duration was adjusted according to the two-1P-period criterion from Section 2.3. The polynomial order was set to quadratic for large wind speeds (12 and 20 m/s) and linear for low wind speeds (8 and 10 m/s). The summary of the input parameter values is given in Table 3.

Recall that the LSF is a comb filter, where all the band-pass replicas have the same frequency response and bandwidth determined by the polynomial order and window length. In contrast to the LSF, the VKF, ODD and proposed method allow each harmonic to adjust independently the frequency response by means of an additional degree-of-freedom (the harmonic bandwidth parameter for the VKF and ODD, and harmonic polynomial order for the proposed). This algorithm feature might be useful in scenarios where a selective harmonic removal is required e.g. closely spaced components with different frequency overlap percentage in the analysis bandwidth. However, this characteristic has not been considered in the present study.

For each signal and method the estimated harmonic perturbation is subtracted from the data, the natural frequency and damping for the principal vibration modes are estimated by the SSI_COV method [1] assuming a 4th order model and relative estimation error with respect to Table 1 is calculated and plotted in Fig. 6. No spectrum stochastic synthesis like (21) or similar has been applied in the present study.

Regarding natural frequency estimation, the LSF, VKF and proposed method exhibit a good performance for both vibration modes. Due to the aforementioned mode-harmonic overlap effect, the error is somewhat larger for a low-speed wind, whilst the estimation improves, as the wind gets stronger. The situation is quite different when it comes to the damping ratio estimation. While the proposed method achieves fairly reasonable estimates for both modes (ranging in 10–30 % for the 1st FA and 10–20 % for the 2nd FA), the reference methods turn to be much less accurate. The LSF presents the largest damping ratio deviations (ranging in 30–50 % for the 1st FA and 50–65 % for the 2nd FA), whilst the VKF estimates are better (ranging in 20–30 % for the 1st FA and 28–55 % for the 2nd FA). When it comes to the ODD only the 1st FA natural frequency estimates come in the neighborhood of the benchmark methods. In turn, it exhibits larger estimation errors especially for low wind speeds. The 2nd FA natural frequency estimates range between roughly 1 % and 2 %, whilst the damping ratio estimates reveal important errors (ranging in 30–60 % for the 1st FA and 30–110 % for the 2nd FA).

The effect of harmonic estimation and subtraction on the residual for the methods is illustrated for the frequency and time domain in Fig. 7 and Fig. 8 respectively (as the LSF returns the sum of harmonics, we have obtained each particular harmonic waveform by means of a set of second order Butterworth filters centered at the harmonic frequencies; in addition, the ODD retrieve no harmonic waveforms and is therefore not represented in Fig. 8). Both LSF and VKF act as a genuine filter, removing large portions of the spectral content in the harmonic analysis bandwidth. This strongly hampers the basic assumption in OMA, that the observed response is the output of a structure to a zero-mean broadband system excitation. In spite of that, the frequency content of the 1st FA is fairly preserved in both methods and thus the good mode characterization returned by the SSI_COV. The situation is rather different regarding the 2nd FA because an important fraction of the mode is removed by the filtering action, which causes the damping ratios to be under-estimated. The interpolation in the harmonic bands in the ODD is highly sensitive to the surroundings spectral content. The uncertainty in the magnitude of the spectral samples often produces a large variance in the interpolation parameters. Moreover, such a procedure yields sharp cut-offs at the band edges, thus rejecting large portions of the power in the neighborhood of the structural modes. Regarding the proposed signal modeling method, the harmonic removal better preserves the overall frequency content of the residual. This is the consequence of the fact that the assumption of linear amplitude and phase evolution in the analysis frame (19) generate modeling inaccuracies in the harmonic bandwidth (the true instantaneous harmonic amplitude and phase might not always have a genuine linear dynamic in the analysis frame). This ensures a robust performance in the neighborhood of lightly damped components (the 2nd FA, in the present) where, due to a small bandwidth, a loss of information can lead to large inaccuracies in damping ratio estimates.

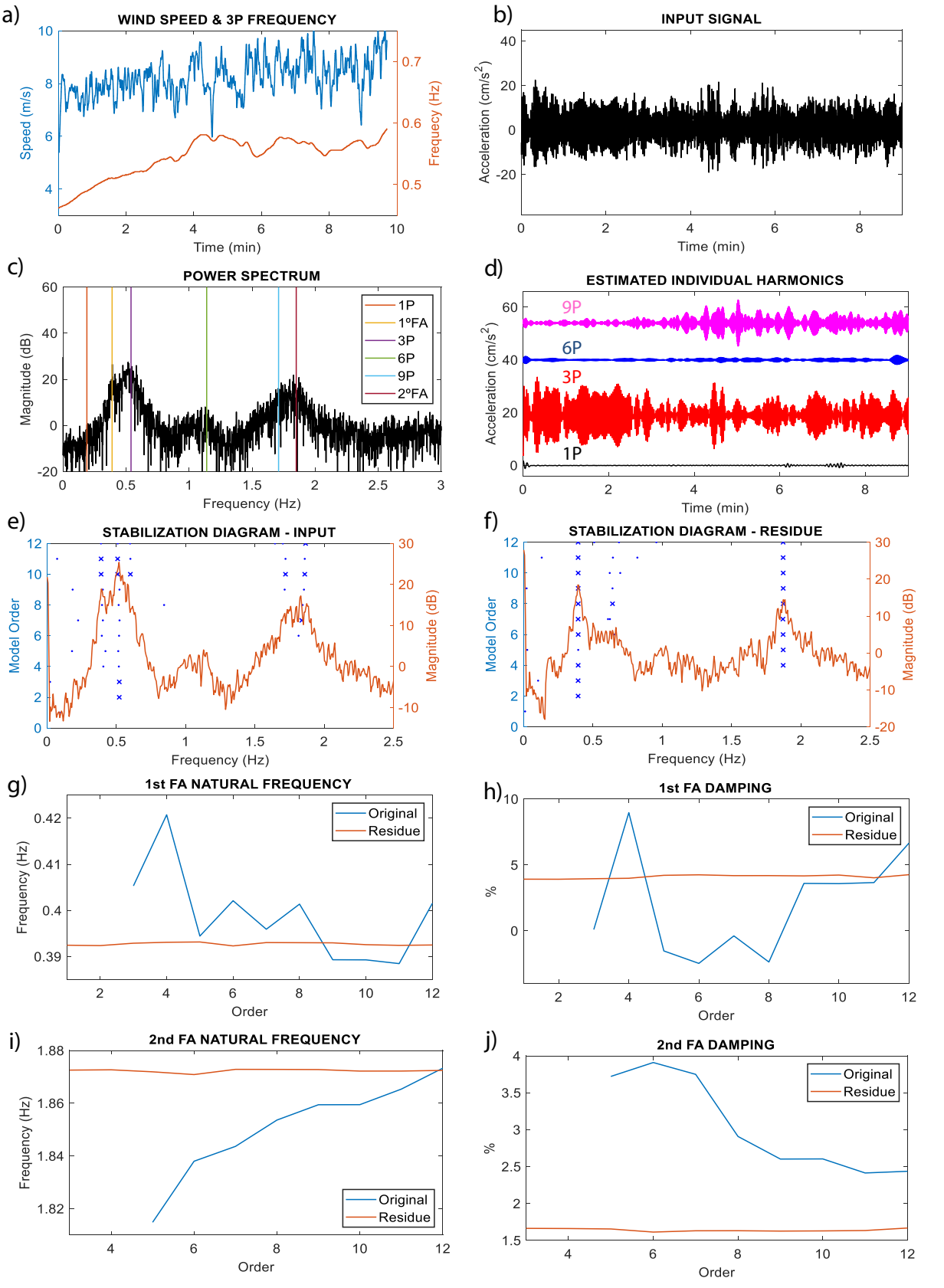

(caption on next page)

Fig. 10. Case study 2 - Raising low speed wind with approximately constant positive slope. The frame length is 11 s and polynomial order equal to 2.

4. Results: real-world case studies

The set of real-world data used to validate the proposed method corresponds to accelerations measured in the nacelle of two 3 MW wind turbines. It contains standard 10-minute records, sampled at 10 ms in the x-axis (wind direction). This accelerometer used for data acquisition was not originally intended for SHM for the following reasons: 1) it is fixed on the wind turbine nacelle instead at appropriate tower heights, 2) only the wind direction accelerations are provided. In spite of these inconveniences, we show next that the proposed method is capable of properly removing the harmonic disturbances from single-channel raw acceleration data. The SCADA (Supervisory Control and Data Acquisition) system also provides the rotating speed of the high-speed shaft, as well as the wind speed measured at the nacelle.

Among a number of data registers processed by the proposed method, we herein present three illustrative cases, which represent different wind speed trends in 10-minute acquisitions from two turbines:

- Case study 1 (CS1): quasi-uniform high-speed wind with considerable amount of turbulence.
- Case study 2 (CS2): raising low speed wind with approximately constant positive slope.
- Case study 3 (CS3): drooping low-speed wind with approximately constant negative slope.

CS1 and CS2 belong to a same turbine (WT1) whereas CS3 describes another turbine (WT2). The only information about the turbines we knew a priori was the approximate values for the principal vibration mode natural frequencies (for 1st FA in range 0.34–0.37 Hz and 2nd FA in range 1.57–1.8 Hz) and that one of the towers exhibited a structural problem. Together with the fact that the data was single-dimension collected from the nacelle, it was quite a challenge to obtain meaningful results.

Each case study is characterized by a figure: CS1- Fig. 9, CS2 – Fig. 10 and CS3 – Fig. 11. The figures have the same internal inlet structure, as explained next.

a) Wind speed (m/s) – acquired by a digital cup anemometer at 20 Hz, located at the nacelle, downstream of the rotor, and 3P rotating frequency (Hz) – measured by a rotary coder at 10 Hz.
b) Input acceleration signal (cm/s^2) – acquired by a sensor device at 100 Hz.
c) Power spectrum of the input acceleration signal shown in the range [0–3] Hz – it contains the principal vibration modes (1st FA and 2nd FA) and rotational harmonics (1P, 3P, 6P, 9P). The vertical lines are located at the values of the vibration modes frequencies, estimated from the stabilization diagram in inlet-f, and average values of the rotational harmonics.
d) Estimated individual harmonic waveforms – these are the individual components in (12) corresponding to 1P, 3P, 6P and 9P. The analysis frame duration used was 10 s (CS1), 11 s (CS2) and 14 s (CS3) according to the criterion from Section 2.3. As for the harmonic frequency, the full-record 3P averaged was used in CS1, whilst for the rest of the cases the measured instantaneous frequency is averaged over the analysis frames.
e) Input signal stabilization diagram – it is calculated from the input acceleration signal by the OoMA Toolbox [60] using the stochastic subspace identification algorithm SSI-COV [1] with the following criteria: 1 % error in frequency, 5 % error in damping, and 98 % confidence in mode shape vectors. The identification algorithm outputs information about stable poles (‘×’) and unstable poles (‘•’) up to a maximum specified model order (equal to 12 in the present study). Vertical alignments of stable poles – stability lines – indicate the presence of vibration modes within the frequency range of analysis.
f) Output signal stabilization diagram – it is calculated from the residual acceleration signal (14) using the same procedure and settings as in inlet-e.

g)–h) 1st FA natural frequency and damping ratio estimates vs model order before (Original) and after (Residue) harmonic removal.
i)–j) 2nd FA natural frequency and damping ratio estimates vs model order before (Original) and after (Residue) harmonic removal.

The stabilization diagrams is a standard tool in OMA for identifying and removing spurious (a.k.a. mathematical) modes from the physical modes of the system under test. If the information about the mode shapes is not available (as it is the case of single-channel data records), the stabilization criteria deal with the natural frequency and damping ratio. It compares the mode characteristics for a given model order to those obtained from a one-order lower model. If a mode appears in most of the models with consistent natural frequency and damping ratio, it is marked as stable, meaning that it is most probably a true physical mode; otherwise, it is labeled as unstable and treated as a spurious mode.

4.1. Case study 1 (CS1)

Our first case study deals with a wind turbine working in the pitch control operation mode (Fig. 9). The wind speed is sustained at about 18 m/s with occasional peaks due to sporadic wind gusts. Accordingly, the measured 3P rotational frequency is very stable at about 0.67 Hz. The power spectrum shows that the harmonics 3P and 9P fall in the neighborhood of the principal vibration modes (1st FA and 2nd FA, respectively). This fact may not be critical for the mode identification as long as the harmonics are (quasi) stationary and thus hardly interfere with the vibration modes. Unfortunately, this is not the case as we observe in inlet-c that the spectral peaks

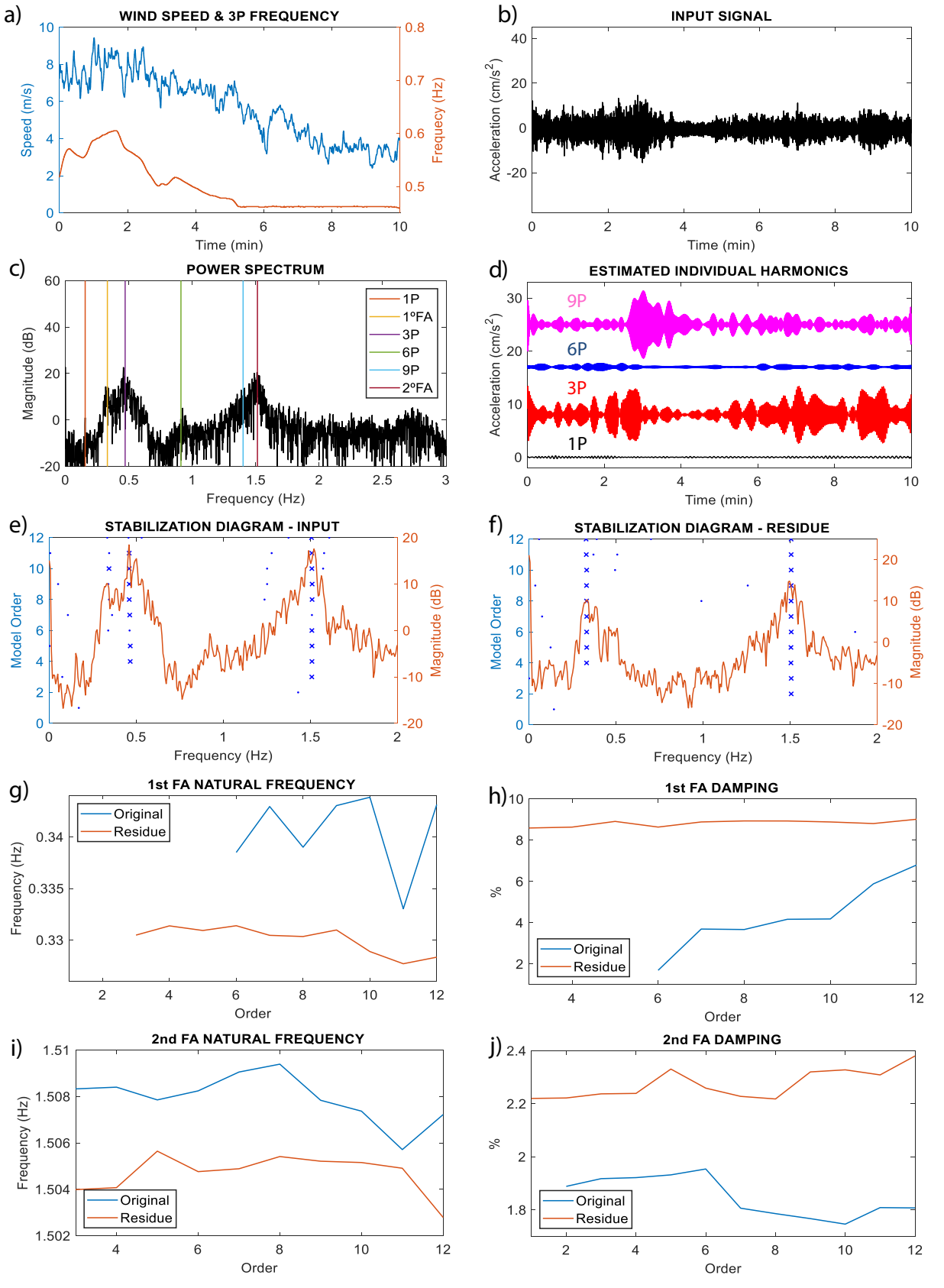

(caption on next page)

Fig. 11. Case study 3 - Drooping low-speed wind with approximately constant negative slope. The frame length is 13 s and polynomial order equal to 2.

exhibit a substantial spread around its average frequencies because of the underlying non-stationarity. At this point, we ignore the exact nature and dynamics of those non-stationarities; however, knowing that the 3P frequency is roughly time-invariant, we expect the harmonic bandwidth (21) to be mostly determined from the instantaneous amplitude. Accordingly, we may expect a considerable amount of interference between the neighboring signal components.

Inlet-d displays the waveforms of the individual estimated harmonics 1P, 3P, 6P and 9P in (12). This inlet is of key importance as it 1) confirms the hypothesis on non-stationary harmonics; 2) shows the dynamics in the instantaneous harmonic amplitude; 3) provides a deeper insight into the contribution of the individual harmonics to the input signal. Accordingly, we observe that 3P and 9P components contribute most to the harmonic perturbation, whilst the impact from 1P and 6P is negligible. What is more, a visual inspection of the waveforms reveals strong and rapid instantaneous amplitude fluctuations, which do not seem to exhibit any particular correlation among them, neither with the wind speed.

The third row in Fig. 9 shows the stabilization diagrams for the input acceleration signal (inlet-e) and residual acceleration signal (inlet-f), the latter obtained by removing the estimated harmonic perturbation from the data (14). In the diagrams appear stable ('×')/unstable ('•') poles, as well as the smoothed power spectrum of the corresponding signal. Regarding the input acceleration signal, only two incomplete stability lines associated to 3P (0.67 Hz) and 2nd FA (1.85 Hz) components appear in the corresponding diagram, whereas 1st FA (0.39 Hz) accounts mostly for unstable poles. It might seem rather curious that,

in spite of a positive visual discrimination 1st FA – 3P from the power spectrum, the SSI-COV algorithm fails to identify the principal vibration mode. On the other hand, this does not really come as a surprise as we know that OMA struggles in analysis scenarios characterized by strong non-stationarities and component interference (collision). As a result, two stability lines clearly stand out at 0.39 Hz (1st FA) and 1.85 Hz (2nd FA) which allows for an accurate identification of the principal natural frequencies, as well as the associated damping factors.

The natural frequency and damping ratio estimates as a function of model order are shown in the bottom rows of Fig. 9. We observe that after removing the harmonics from the original data, the estimates become much more concentrated in both parameters. We cannot discuss the damping ratio estimates, due to the lack of a priori information; nevertheless, the values seem plausible because they are situated roughly around the average of the large-deviation estimates from the original input data.

4.2. Case study 2 (CS2)

This case (Fig. 10) describes the operation of the same wind turbine as in CS1 in the torque-control operation mode (between cut-in and rated wind speed). The blade pitch is constant whereas the generator torque is varying, so that both the blade tip speed and rotor speed increase proportionally to the wind speed [61]. The wind speed is slowly increasing, which might not be immediately evident because of the inlet-a y-axis scaling. Nevertheless, the 3P frequency is clearly increasing as well. Similar to CS1, the power spectrum shows frequency locations of the principal vibration modes and harmonic components. Again, a substantial energy dispersion around average harmonic frequencies, due to the presence of non-stationarities, is clearly visible; moreover, observe in inlet-e that visual identification of 1st FA is hampered by the fact that 3P harmonic dominates low-frequency spectrum. As the 3P frequency is gradually changing, it is clear that the harmonic bandwidth (21) will be determined by the combined dynamics of both the instantaneous amplitude and phase.

The estimated individual harmonics are shown in inlet-d. 3P harmonic is evidently the most prominent, followed by 9P harmonic. Like in CS1, we cannot discuss the morphology of the individual harmonic waveforms, as we are not acquainted with the mechanical actions that yield such an outcome. Nevertheless, we can verify that these waveforms do not resemble those generated by a sustained wind forcing (CS1).

The stabilization diagram of the data completely fails in identifying stable vibration modes. Once more, this case study illustrates the fact that the SSI-COV is seriously jeopardized by the presence of non-stationarities in data, as well as colliding components. The suppression of the estimated harmonics from the data delivers the residue, whose stabilization diagram shows two stability lines located at the frequencies of the principal vibration modes: 0.39 Hz (1st FA) and 1.85 Hz (2nd FA). Furthermore, inlets-g to –j show a consistency in the principal mode parameter estimates with CS1.

4.3. Case study 3 (CS3)

Fig. 11 characterizes the third case study, which describes a different wind turbine (WT2) operating in the below-rated region. Unlike CS2, here the turbine progressively reduces the rotation speed as the wind speed drops with almost constant rate of about −0.57 m/s per minute. The 3P is decreasing accordingly around the cut-in limit after 5.5 min approximately, when the wind speed falls below 5 m/s. At this point, the control system keeps the rotor speed nearly constant.

Compared to the previous case studies, the input data exhibits smaller acceleration values; in a like manner, the power spectrum magnitude drops accordingly. Observe that, in the present case study, the position of the principal vibration modes is 0.33 Hz (1st FA) and 1.51 Hz (2nd FA). As the rotation speed is decreasing, it is to expect that both instantaneous amplitude and phase will contribute to the harmonic bandwidth (21). In the corresponding spectrogram, we observe that the 3P harmonic's energy level is especially significant around the beginning and end of the data recording. On the contrary, the 1st FA exhibits an important energy spread for the

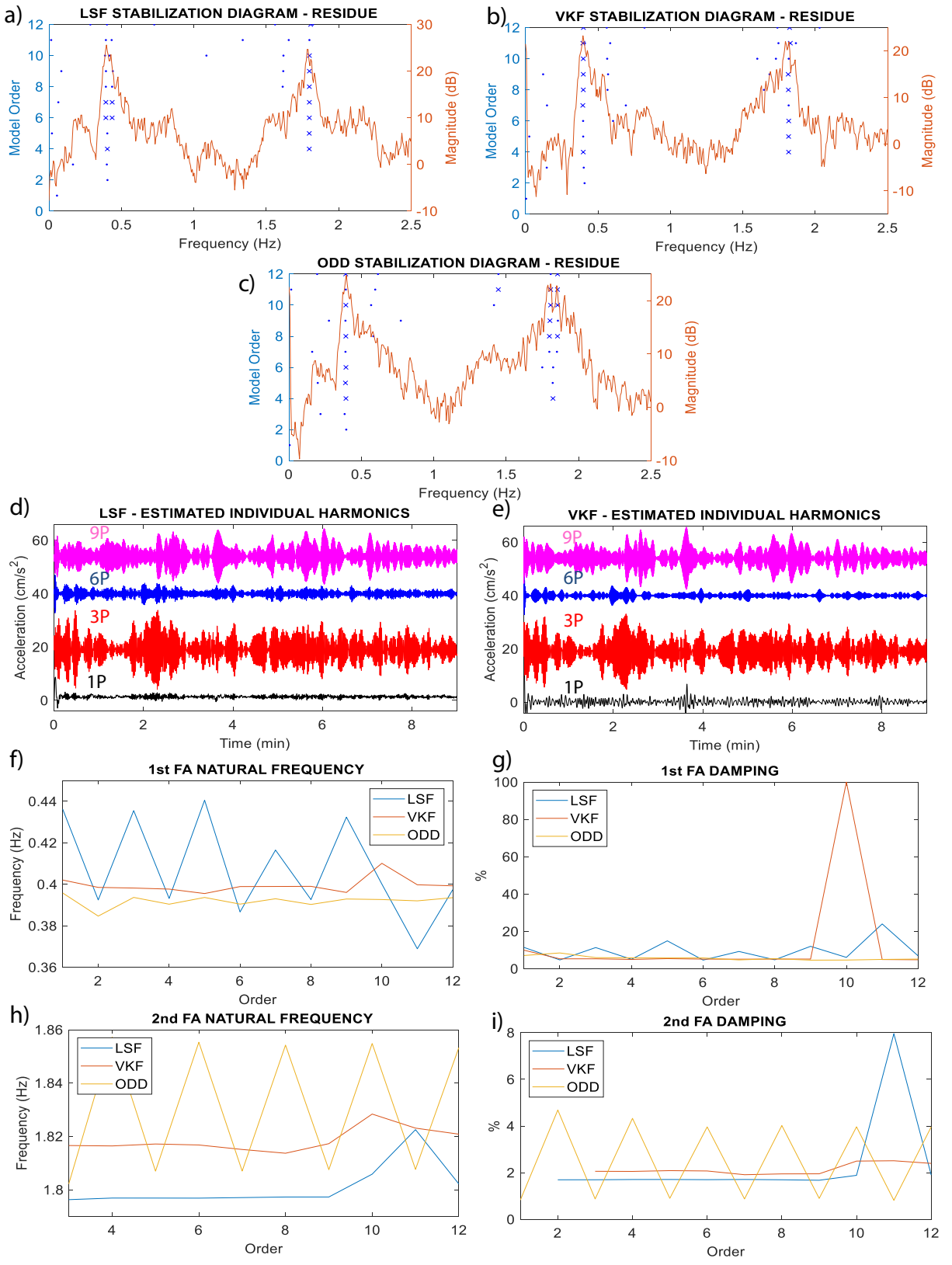

Fig. 12. Case study 1 – Results for the LSF, VKF and ODD methods. LSF: window length equal to 7 and order equal to 3. VKF: bandwidth equal to 0.18 Hz and order equal to 2. ODD: bandwidth 0.18 Hz – linear interpolation.

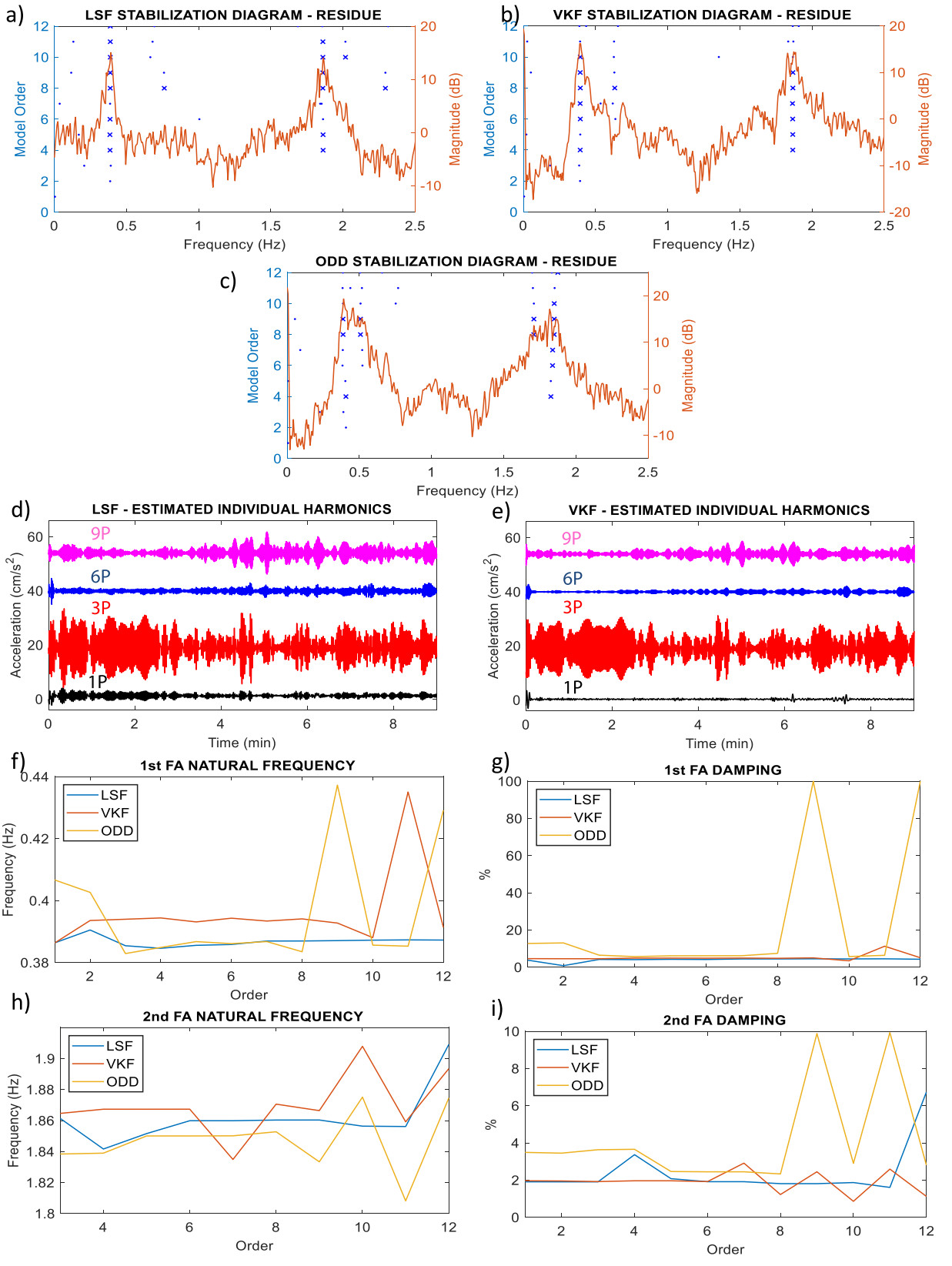

(caption on next page)

Fig. 13. Case study 2 – Results for the LSF, VKF and ODD methods. LSF: window length equal to 5 and order equal to 3. VKF: bandwidth equal to 0.16 Hz and order equal to 2. ODD: bandwidth 0.16 Hz – linear interpolation.

whole duration of the data, as a consequence of the interaction with the 3P harmonic.

This is supported by the estimated individual harmonic waveforms where we observe a drop in 3P instantaneous amplitude around the middle of the data recording. 3P and 9P harmonic waveforms reveal quite different energy time distribution, although their overall energy is similar. Analogous to the previous case studies, the contribution from 1P and 6P is negligible.

In the stabilization diagram of the input data, two stability lines are found at 0.47 Hz (3P) and 1.51 Hz (2nd FA). Thus, OMA successfully detects the second vibration mode but fails to capture 1st FA. On the contrary, the smoothed power spectrum of the residue shows that the harmonic removal resolves the spectral clusters around the 1st FA, which in turn yields two stability lines at 0.33 Hz (1st FA) and 1.51 Hz (2nd FA). Similar to the previous case studies, the algorithm delivers very stable estimates vs model order. Note, however, that there is a certain mismatch between the initial guess about the 2nd FA natural frequency and its estimate, which we believe stem from the known tower structural problem.

4.4. LSF, VKF and ODD in the context of real signals

In order to check the performance of the LSF, VKF and ODD in the real wind turbine signals, we have incorporated the information about instantaneous 3P frequency measurement in all the algorithms: in the LSF and ODD by resampling the data in the angular domain and in the VKF by calculating the instantaneous phase for the filter structure equation. The input parameters for all the algorithms have been adjusted following the same criteria as in Section 3.2. In particular, for the LSF the order was set to 3 and window length to 7 cycles. For the VKF the order was set to 2 and bandwidth to 0.17 Hz; the same bandwidth was used for the ODD whilst the interpolation mode was set to linear.

Finally, for the proposed method the order was set to 2 and the frame length to 2 1P cycles. Moreover, the stochastic spectrum synthesis (21) has been applied to both methods.

We have analyzed the three case study data and we show in Figs. 12 – 14 respectively the results when applied to the LSF, VKF and ODD. For all the cases the stabilization diagrams show that for LSF and VKF methods the principal vibration modes are detected. However, in some cases the stabilization diagram also exhibits a closely-spaced double column of stable poles, which appears around the vibration modes (for example, Fig. 12 inlet-a). This effect is a consequence of a partially resolved mode-harmonic collision problem, which means that a fraction of the harmonic energy is still present in the analysis bandwidth. Similar conclusions can be drawn for the ODD results e.g. a closely-spaced double column of stable poles for the 2nd FA in Figs. 12, 13 and14 inlet-c. In addition, in CS1 and CS2 the 1st FA is hardly detected (Fig. 12 and Fig. 13 inlet-c), because the method is seriously degraded when dealing with strongly overlapped components.

The estimated harmonic waveforms roughly resemble those obtained by the proposed method, although eye-catching differences appear in 1P and 9P waveforms (we recall that the ODD cannot extract the harmonic waveforms). The large variance in the 1P waveform estimated by the LSF (for example Fig. 13 inlet-d) comes from the low-pass comb filter effect (the method does not filter around the 1P frequency; it removes the spectral content below the 1st FA). The low-variance 9P waveform estimated the VKF (for example Fig. 13 inlet-e) corroborates the aforementioned argumentation on the unresolved closely-spaced components. Similar examples could be found elsewhere in Figs. 12 – 14 by a visual inspection.

Furthermore, we show on inlet-f through –i, the principal vibration mode parameter estimation for the benchmark methods. We see that the estimates for all the methods fall roughly in the same range as for the proposed method. However, unlike the proposed method, which yields a consistent parameter estimates over the increasing model order, the LSF, VKF and ODD estimates manifest an erratic/fluctuating behavior. Moreover, the mean of the estimates partially matches only for the damping ratios, whilst there is a mismatch for the natural frequencies. Such estimates might seriously hamper the SHM, where consistent vibration mode parameter estimates across 10-min data registers are needed to ensure a proper wind turbine mechanical structure supervision.

5. Conclusions

As the main conclusion of our work, we can say that the method proposed in this paper is highly effective in removing the influence of the harmonics in acceleration data acquired from the tower of a wind turbine, while keeping intact the information required to properly calculate the structural vibration modes. This affirmation is validated by a parameter sensitivity analysis, a comparative study involving three state-of-the-art methods on synthetic data and a number of real-world experimental tests, from which we have selected the three illustrative cases, corresponding to different operation regimes. It is important to stress that the signals taken from sensors at the nacelle were not intended to perform structural health monitoring (SHM); therefore, the presence of the harmonics in the data has rendered the analysis scenario far more complex.

The chief benefit of our approach is that it deals with non-stationarities in the harmonics in both amplitude and phase, delivering quality principal vibration mode parameter estimates even in presence of strong component interference. In real data, we have used the information of the rotation speed provided by the SCADA, sampled at 100 ms, but we have also estimated instantaneous frequency/phase variations. This means that the algorithm could also work with an initial guess of the rotations speed, and then update its value from the estimated phase. In addition, the algorithm has also obtained an estimate of the harmonic instantaneous amplitude.

We have shown through a benchmark study that when only the average rotational speed is known, the proposed method

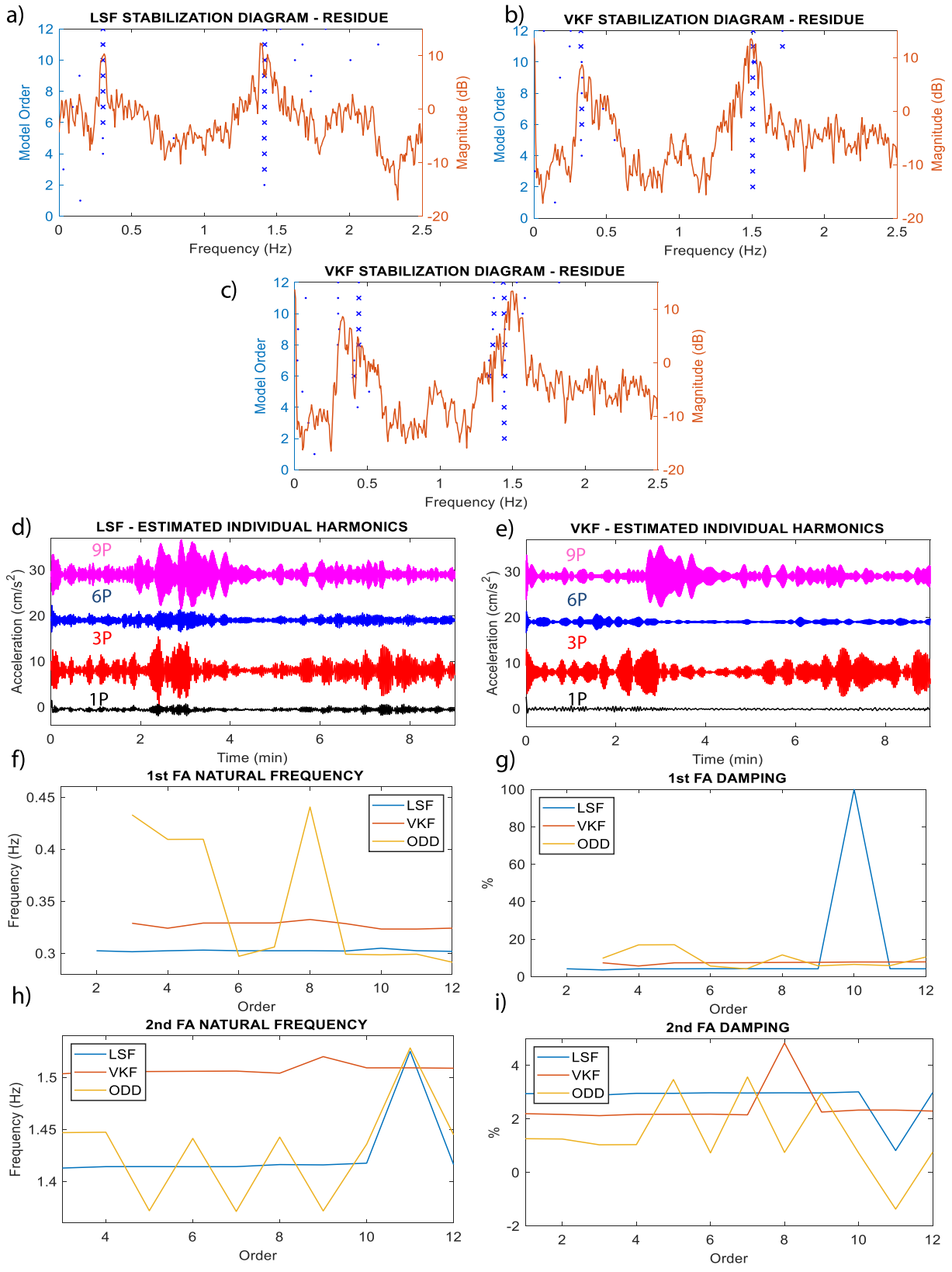

Fig. 14. Case study 3 – Results for the LSF, VKF and ODD methods. LSF: window length equal to 5 and order equal to 3. VKF: bandwidth equal to 0.16 Hz and order equal to 2. ODD: bandwidth 0.16 Hz – linear interpolation.

outperforms the reference state-of-the art methods, in terms of structural mode parameter estimation relative error. In real wind turbine data analysis scenarios where instantaneous rotational speed can be delivered by a measurement device, the proposed method yields consistent parameter estimates, which can readily be used for SHM. The LSF, VKF and ODD yielded inconsistent estimates which also incorporated certain fluctuation dynamics.

The fact that we have introduced a precise non-stationary model for all relevant harmonics allows not only removing them from the original signal, but also obtain information about the harmonics themselves, and eventually, we believe, information of the system. For instance, it seems noteworthy to us that there seems not to exist any correlation between wind speed and the 3P harmonic. Much in the same way, the harmonic envelopes, and therefore the instantaneous power of the different harmonics exhibit seemingly unrelated time patterns. These observations suggest a deeper analysis to find out what kind of factors, external or internal, influence the characteristics of the harmonics, and if they contain information on the structure (or, perhaps, the wind) which may be useful to determine possible failures in the turbine mechanical structure. This is an open area for future research.

Declaration of Competing Interest

The authors declare that they have no known competing financial interests or personal relationships that could have appeared to influence the work reported in this paper.

Data availability

The data that has been used is confidential.

Acknowledgements

This work has been supported by the Spanish Research Agency under grant AEI/FEDER, PID2019-107258RB-C32, and also by the Government of Navarre (Dpt. Of Economic and Business Development) under grant 0011-1365-2021-000159.

References

[1] E. Reynders, System identification methods for (operational) modal analysis: review and comparison, Arch. Comput. Methods Eng. 19 (2012) 51–124.
[2] F. Magalhães, A. Cunha, Explaining operational modal analysis with data from an arch bridge, Mech. Syst. Signal Process. 25 (2011) 1431–1450.
[3] N.-J. Jacobsen, P. Andersen, R. Brincker, Eliminating the influence of harmonic components in operational modal analysis, in: Conf. Proc. IMAC-XXIV A Conf. Expo. Struct. Dyn., Society for Experimental Mechanics, 2007.
[4] D. Abboud, Y. Marnissi, A. Assoumane, Y. Hawwari, M. Elbadaoui, Synchronous analysis of cyclo-non-stationary signals: a comprehensive study with aeronautic applications, Mech. Syst. Signal Process. 168 (2022), 108600, https://doi.org/10.1016/j.ymssp.2021.108600.
[5] J.L. Dion, I. Tawfiq, G. Chevallier, Harmonic component detection: optimized Spectral Kurtosis for operational modal analysis, Mech. Syst. Signal Process. 26 (2012) 24–33, https://doi.org/10.1016/j.ymssp.2011.07.009.
[6] S. Greś, M. Döhler, P. Andersen, L. Mevel, Kalman filter-based subspace identification for operational modal analysis under unmeasured periodic excitation, Mech. Syst. Signal Process. 146 (2021), 106996.
[7] G.H. James III, T.G. Carne, J.P. Lauffer, J.P. Lauffer, The natural excitation technique (NExT) for modal parameter extraction from operating wind turbines, Int. J. Anal. Exp. Modal Anal. 10 (1993) 260–277.
[8] K. Motte, W. Weijtjens, C. Devriendt, P. Guillaume, Operational modal analysis in the presence of harmonic excitations: a review, Dyn. Civ. Struct. 2 (2015) 379–395.
[9] S. Manzato, D. Moccia, B. Peeters, K. Janssens, J.R. White, A review of harmonic removal methods for improved operational modal analysis of wind turbines, Int. Conf. Noise Vib. Eng. 2012, ISMA 2012, Incl. USD 2012 Int. Conf. Uncertain. Struct. Dyn. 4 (2012) 2675–2689.
[10] S. Manzato, C. Devriendt, W. Weijtjens, E. Di Lorenzo, B. Peeters, P. Guillaume, Removing the influence of rotor harmonics for improved monitoring of offshore wind turbines, Conf. Proc. Soc. Exp. Mech. Ser. 4 (2014) 299–312, https://doi.org/10.1007/978-3-319-04546-7_34.
[11] A.A.W. van Vondelen, S.T. Navalkar, A. Iliopoulos, D.C. van der Hoek, J.-W. van Wingerden, Damping identification of offshore wind turbines using operational modal analysis: a review, Wind Energy Sci. 7 (2022) 161–184, https://doi.org/10.5194/wes-7-161-2022.
[12] B. Peeters B. Cornelis K. Janssens H. Van der Auweraer Removing disturbing harmonics in operational modal analysis Proc. Int. Oper. Modal Anal. Conf 2007 Copenhagen, Denmark.
[13] S. Braun, The synchronous (time domain) average revisited, Mech. Syst. Signal Process. 25 (2011) 1087–1102, https://doi.org/10.1016/j.ymssp.2010.07.016.
[14] D. Tcherniak, S. Chauhan, M.H. Hansen, Applicability limits of operational modal analysis to operational wind turbines, Conf. Proc. Soc. Exp. Mech. Ser. 1 (2011) 317–327, https://doi.org/10.1007/978-1-4419-9716-6_29.
[15] A. Brandt, A signal processing framework for operational modal analysis in time and frequency domain, Mech. Syst. Signal Process. 115 (2019) 380–393.
[16] H.A. Cole, on-Line Failure Detection and Damping Measurement of Aerospace Structures By Random Decrement Signatures., NASA Contract. Reports. (1973).
[17] C. Brincker, R. Ventura, Introduction to Operational Modal Analysis, Wiley, 2021.
[18] J.K. Vandiver, A.B. Dunwoody, R.B. Campbell, M.F. Cook, A mathematical basis for the random decrement vibration signature analysis technique, (1982).
[19] C.S. Huang, C.H. Yeh, Some properties of Randomdec signatures, Mech. Syst. Signal Process. 13 (1999) 491–507, https://doi.org/10.1006/mssp.1998.0194.
[20] S.V. Modak, Separation of structural modes and harmonic frequencies in Operational Modal Analysis using random decrement, Mech. Syst. Signal Process. 41 (2013) 366–379.
[21] R.B. Randall, B. Peeters, J. Antoni, S. Manzato, New cepstral methods of signal preprocessing for operational modal analysis, in: Proc. Int. Conf. Noise Vib. Eng., 2012.
[22] R.B. Randall, M.D. Coats, W.A. Smith, Repressing the effects of variable speed harmonic orders in operational modal analysis, Mech. Syst. Signal Process. 79 (2016) 3–15, https://doi.org/10.1016/j.ymssp.2016.02.042.
[23] F. Liu, J. Wang, M. Li, F. Gu, A.D. Ball, Operational modal analysis in the presence of pulse train and harmonics based on SSI, in: Adv. Asset Manag. Cond. Monit., Springer, 2020: pp. 115–134.
[24] R.B. Randall, N. Sawalhi, M. Coats, A comparison of methods for separation of deterministic and random signals, Int. J. Cond. Monit. 1 (2011) 11–19, https://doi.org/10.1784/204764211798089048.
[25] S. Manzato, J.R. White, B. LeBlanc, B. Peeters, K. Janssens, Advanced identification techniques for operational wind turbine data, Conf. Proc. Soc. Exp. Mech. Ser. 45 (2014) 195–209, https://doi.org/10.1007/978-1-4614-6585-0_19.

[26] R. Brincker, P. Andersen, N. Moller, Indicator for separation of structural and harmonic modes in output-only modal testing, Proc. Int. Modal Anal. Conf. - IMAC. 2 (2000) 1649–1654.
[27] D. Tcherniak, Detection and identification of a damaged blade using only a tower sensor, without stopping the wind turbine, in: Proc. ISMA 2016 - Int. Conf. Noise Vib. Eng. USD2016 - Int. Conf. Uncertain. Struct. Dyn., KU Leuven, Departement Werktuigkunde, 2016: pp. 4097–4109.
[28] T.-P. Le, P. Argoul, Distinction between harmonic and structural components in ambient excitation tests using the time–frequency domain decomposition technique, Mech. Syst. Signal Process. 52 (2015) 29–45.
[29] A. Agneni, G. Coppotelli, C. Grappasonni, A method for the harmonic removal in operational modal analysis of rotating blades, Mech. Syst. Signal Process. 27 (2012) 604–618.
[30] A.A.W. van Vondelen, A. Iliopoulos, S.T. Navalkar, D.C. van der Hoek, J.-W. van Wingerden, Damping Identification of an Operational Offshore Wind Turbine using Enhanced Kalman filter-based Subspace Identification, (2022) 1–19.
[31] S. Qian, Gabor expansion for order tracking, Sound Vib. 37 (2003) 18–23.
[32] C. Devriendt, P. Guillaume, The use of transmissibility measurements in output-only modal analysis, Mech. Syst. Signal Process. 21 (2007) 2689–2696.
[33] C. Devriendt, P. Guillaume, Identification of modal parameters from transmissibility measurements, J. Sound Vib. 314 (2008) 343–356, https://doi.org/10.1016/j.jsv.2007.12.022.
[34] C. Devriendt, G. De Sitter, S. Vanlanduit, P. Guillaume, Operational modal analysis in the presence of harmonic excitations by the use of transmissibility measurements, Mech. Syst. Signal Process. 23 (2009) 621–635.
[35] W. Weijtjens, J. Lataire, C. Devriendt, P. Guillaume, Dealing with periodical loads and harmonics in operational modal analysis using time-varying transmissibility functions, Mech. Syst. Signal Process. 49 (2014) 154–164, https://doi.org/10.1016/j.ymssp.2014.04.008.
[36] P.-J. Daems, C. Peeters, P. Guillaume, J. Helsen, Removal of non-stationary harmonics for operational modal analysis in time and frequency domain, Mech. Syst. Signal Process. 165 (2022), 108329.
[37] S. Baudin, J. Antoni, D. Rémond, O. Sauvage, Excitation/transfer separation in non-stationary conditions, in: Surveill. 7 Int. Conf., 2013: pp. 1–10.
[38] J. Berntsen, A. Brandt, Periodogram ratio based automatic detection and removal of harmonics in time or angle domain, Mech. Syst. Signal Process. 165 (2022), 108310.
[39] P. Mohanty, D.J. Rixen, Operational modal analysis in the presence of harmonic excitation, J. Sound Vib. 270 (2004) 93–109, https://doi.org/10.1016/S0022-460X(03)00485-1.
[40] P. Mohanty, D.J. Rixen, Modified ERA method for operational modal analysis in the presence of harmonic excitations, Mech. Syst. Signal Process. 20 (2006) 114–130.
[41] X. Dong, J. Lian, M. Yang, H. Wang, Operational modal identification of offshore wind turbine structure based on modified stochastic subspace identification method considering harmonic interference, J. Renew. Sustain. Energy. 6 (2014) 1–29, https://doi.org/10.1063/1.4881876.
[42] S. Gres, P. Andersen, C. Hoen, L. Damkilde, Orthogonal projection-based harmonic signal removal for operational modal analysis, Conf. Proc. Soc. Exp. Mech. Ser. 6 (2019) 9–21, https://doi.org/10.1007/978-3-319-74476-6_2.
[43] S. Gres, P. Andersen, L. Damkilde, Operational modal analysis of rotating machinery, Conf. Proc. Soc. Exp. Mech. Ser. (2019) 67–75, https://doi.org/10.1007/978-3-319-74693-7_7.
[44] E. Smilden, A. Sørensen, L. Eliassen, Wind model for simulation of thrust variations on a wind turbine, Energy Procedia 94 (2016) 306–318.
[45] A. Lazkano, K. Redondo, P. Saiz, J.J. Gutierrez, I. Azcarate, L.A. Leturiondo, J. Barros, Case study: Flicker emission and 3P power oscillations on fixed-speed wind turbines, in: 2012 IEEE 15th Int. Conf. Harmon. Qual. Power, IEEE, 2012: pp. 268–273.
[46] X. Serra, Musical sound modeling with sinusoids plus noise, Music. Signal Process. (1997) 91–122.
[47] Y. Stylianou, Applying the harmonic plus noise model in concatenative speech synthesis, IEEE Trans. Speech Audio Process. 9 (2001) 21–29.
[48] M. Zivanovic, J. Schoukens, Single and piecewise polynomials for modeling of pitched sounds, IEEE Trans. Audio, Speech Lang. Process. 20 (2012), https://doi.org/10.1109/TASL.2011.2174228.
[49] M. Zivanovic, J. Schoukens, On the polynomial approximation for time-variant harmonic signal modeling, IEEE Trans. Audio, Speech Lang. Process. 19 (2011), https://doi.org/10.1109/TASL.2010.2049673.
[50] W. Verhelst, Overlap-add methods for time-scaling of speech, Speech Commun. 30 (2000) 207–221, https://doi.org/10.1016/S0167-6393(99)00051-5.
[51] H. Vold, J. Leuridan, High resolution order tracking at extreme slew rates, using Kalman tracking filters, SAE Technical Paper, 1993.
[52] J. Tuma, Setting the passband width in the Vold-Kalman order tracking filter, in: 12th Int. Congr. Sound Vib., 2005: pp. 1–8.
[53] M.C. Pan, C.X. Wu, Adaptive Vold-Kalman filtering order tracking, Mech. Syst. Signal Process. 21 (2007) 2957–2969, https://doi.org/10.1016/j.ymssp.2007.06.002.
[54] M.C. Pan, W.C. Chu, D. Do Le, Adaptive angular-velocity Vold-Kalman filter order tracking-Theoretical basis, numerical implementation and parameter investigation, Mech. Syst. Signal Process. 81 (2016) 148–161, https://doi.org/10.1016/j.ymssp.2016.03.013.
[55] L. Cohen, Time-frequency Analysis, Prentice Hall PTR, Englewood Cliffs, NJ, 1995.
[56] J.M. Jonkman, M.L. Buhl, FAST user's guide, National Renewable Energy Laboratory Golden, CO, USA, 2005.
[57] J. Jonkman, S. Butterfield, W. Musial, G. Scott, Definition of a 5-MW reference wind turbine for offshore system development, National Renewable Energy Lab. (NREL), Golden, CO (United States), 2009.
[58] G. Bir, J. Jonkman, Aeroelastic instabilities of large offshore and onshore wind turbines, J. Phys. Conf. Ser., IOP Publishing (2007) 12069.
[59] K. Stol, H.-G. Moll, G. Bir, H. Namik, A comparison of multi-blade coordinate transformation and direct periodic techniques for wind turbine control design, in: 47th AIAA Aerosp. Sci. Meet. Incl. New Horizons Forum Aerosp. Expo., 2009: p. 479.
[60] A. Otto, OoMA Toolbox, (2021). https://www.mathworks.com/matlabcentral/fileexchange/68657-ooma-toolbox.
[61] J. Aho, A. Buckspan, J. Laks, P. Fleming, Y. Jeong, F. Dunne, M. Churchfield, L. Pao, K. Johnson, A tutorial of wind turbine control for supporting grid frequency through active power control, Am. Control Conf., IEEE 2012 (2012) 3120–3131.